

Primary frequency control in isolated power grids

Pedro Miguel Barros dos Santos

Thesis to obtain the Master of Science Degree in

Electrical and Computer Engineering

Supervisor: Prof. José Manuel Dias Ferreira de Jesus

Examination Committee

Chairperson: Prof^a. Maria Eduarda de Sampaio Pinto de Almeida Pedro

Supervisor: Prof. José Manuel Dias Ferreira de Jesus

Members of the Committee: Prof. Luís António Fialho Marcelino Ferreira

October 2014

Abstract

Satisfactory operation of a power system is predominantly assured by keeping voltage levels and frequency in narrow tolerance bands. As any other system, a power system is frequently subject to changes in operating conditions, which find their cause in faults or the loss of a major generating unit. With the goal of controlling the two variables, specific devices are often equipped in generating units. Frequency regulation, the topic covered in this work, is directly related to the active power balance in the system. In order for a unit to be able to control its mechanical power and consequently system frequency, a device called a speed governor is installed. Performance of said speed governors varies widely depending on the type of resource a power plant is based on. The usual practice in power systems is to rely on thermal power plants to conduct primary frequency control, especially in isolated or weaker grids where few generators exist.

The core objective of this thesis is to determine to what degree hydroelectric power plants can contribute to primary frequency regulation in isolated grids. This goal is achieved by first defining the relevant dynamic models of hydraulic turbines and speed governors and then establishing parameter requirements that lead to optimum governor performances. Lastly, transient stability simulations are performed in order to form a conclusion about the influence of hydroelectric speed governing in system frequency control.

Keywords: Transient Stability, Dynamic Models, Turbine-Governor Systems, Speed Governor Tuning

Resumo

O funcionamento satisfatório do sistema de energia eléctrica é principalmente assegurado através da manutenção dos níveis de tensão e frequência em limites próprios. Este sistema é constantemente objecto de alterações nas suas condições de funcionamento, sendo as suas causas a ocorrência de falhas eléctricas ou a perda de um grupo de geração de dimensão considerável. Com o intuito de controlar as duas variáveis, dispositivos adequados são tendencialmente instalados nas unidades de geração. A regulação de frequência, tema abordado neste trabalho, está directamente relacionada com o balanço de potência activa na rede. Fazendo jus ao objectivo de um grupo gerador controlar a sua potência mecânica e conseqüentemente a frequência da rede, um dispositivo denominado regulador de velocidade é instalado. O desempenho destes reguladores é substancialmente diferente consoante o tipo de recurso energético usado por uma central eléctrica. A prática comum nos sistemas de energia dita que o controlo primário de frequência é assegurado pelos grupos térmicos das centrais, especialmente em redes mais fracas.

A meta a atingir com esta dissertação é a de determinar até que grau as centrais hidroeléctricas contribuem para a regulação primária de frequência em redes. Para tal, e numa fase inicial, definem-se modelos dinâmicos relevantes de turbinas hidráulicas e seus reguladores de velocidade, para de seguida estabelecer requisitos de parâmetros que conduzam a desempenhos óptimos dos reguladores. Em modo de finalização, estudos de estabilidade transitória são executados com o intuito de concluir acerca do impacto dos reguladores de velocidade hidroeléctricos no controlo da frequência do sistema.

Palavras-chave: Estabilidade Transitória, Modelos Dinâmicos, Reguladores Carga-Velocidade, Parametização Regulador Carga-Velocidade

Table of Contents

Abstract.....	iii
Resumo	v
Table of Contents	vii
Index of Figures.....	ix
Index of Tables	xi
List of Symbols	xiii
Chapter 1 - Introduction.....	1
1.1 Context and Motivation.....	1
1.2 Objectives	2
1.3 Thesis Outline.....	2
Chapter 2 - Hydraulic Turbines and Governing Systems.....	3
2.1 Generalities	3
2.2 Modelling	5
2.2.1 Hydraulic Turbines.....	5
2.2.2 Speed Governors	9
Chapter 3 - Case Study Network.....	15
3.1 Network Composition	15
3.2 Power Flow Results.....	15
3.2.1 Summer Peak.....	16
3.2.2 Winter Valley	17
3.3 Dynamic Models	19
Chapter 4 - Hydraulic Speed Governor Tuning.....	23
4.1 Linear Model Analysis	23
4.2 HYGGOV Model Analysis	29
Chapter 5 - Network Dynamic Simulations.....	35
5.1 Foros 60kV/30kV Transformer Fault	35
5.2 Pico Vermelho Contingency	37
5.2.1 Summer Peak.....	37
5.2.2 Winter Valley	39

5.3 Caldeirão Unit 5 Contingency.....	43
5.4 Caldeirão Unit 6 Transformer Contingency	45
5.5 Pelton vs Francis Performance	48
Chapter 6 - Conclusion.....	49
6.1 Thesis Discussion.....	49
6.2 Future Work.....	50
Bibliography	51
Appendix A – Grid schematic	53

Index of Figures

Figure 2.1 – Schematic of a hydroelectric power plant [1]. 3

Figure 2.2 – Pelton Turbine. 4

Figure 2.3 – Francis turbine..... 4

Figure 2.4 – Functional block diagram of hydraulic turbine generating system [1]. 5

Figure 2.5 – Hydraulic turbine nonlinear model assuming inelastic water column [4]. 6

Figure 2.6 – Relationship between ideal and real gate positions [1]..... 8

Figure 2.7 – Linear turbine model with inelastic water column [4]. 8

Figure 2.8 – Turbine power change due to a unit step gate opening [1]..... 9

Figure 2.9 – Hydraulic plant governing system schematic [3]. 10

Figure 2.10 – Ideal steady state characteristic of governor with speed droop [1]. 10

Figure 2.11 - Mechanical-Hydraulic governor for hydro turbine [5]. 11

Figure 2.12 – Hydraulic turbine governor model [6]. 13

Figure 2.13 – Block diagram of linear governing system [1]. 13

Figure 4.1 – Hydraulic unit speed governor block diagram..... 23

Figure 4.2 – Governor time simulations for a unit with $TW = 2,0$ and $TM = 6,0$ 25

Figure 4.3 – Constant damping ratio locus for a unit with $TW = 2,0$ and $TM = 6,0$ 26

Figure 4.4 - Constant time constant of mode 2 locus for a unit with $TW = 2,0$ and $TM = 6,0$ 27

Figure 4.5 - Constant time constant of mode 3 locus for a unit with $TW = 2,0$ and $TM = 6,0$ 27

Figure 4.6 - Constant damping ratio locus for a unit with $TW = 1,0$ and $TM = 6,0$ 27

Figure 4.7 - Constant damping ratio locus for a unit with $TW = 1,0$ and $TM = 4,0$ 27

Figure 4.8 - Constant damping ratio locus for a unit with $TW = 3,0$ and $TM = 6,0$ 28

Figure 4.9 – Nonlinear HYGGOV model block diagram [8]. 29

Figure 4.10 – Time simulations of speed for a unit with $TM = 2 \times 1,435$ and $TW = 0,89$ 30

Figure 4.11 – Time simulations of mechanical power for a unit with $TM = 2 \times 1,435$ and $TW = 0,89$. 30

Figure 4.12 – Optimum dynamic speed responses for two cases. 32

Figure 4.13 – Effect of unit parameter TM in speed governor response..... 33

Figure 4.14 – Speed governor responses of hydro and thermal units. 34

Figure 5.1 – Frequency response on the 60kV bus of the Caldeirão power plant for the Foros transformer fault. CTCL6 (A) – HYGGOV considered. CTCL6 (B) – HYGGOV not considered..... 36

Figure 5.2 – Mechanical power response of the Caldeirão Unit 5 and the Furnas Unit 1 for the Foros transformer fault. GCHRF (A) and G5CTCL (A) – HYGGOV considered. GCHRF (B) and G5CTCL (B) – HYGGOV not considered. 37

Figure 5.3 – Frequency response on the 60kV bus of the Caldeirão power plant for the Pico Vermelho contingency. CTCL6 (A) – HYGGOV considered with load shedding ON. CTCL6 (B) – HYGGOV not considered with load shedding ON. CTCL6 (C) – HYGGOV considered with load shedding OFF. CTCL6 (D) – HYGGOV not considered with load shedding OFF..... 38

Figure 5.4 – Frequency response on the 60kV bus of the Caldeirão power plant for the Pico Vermelho contingency. CTCL6 (A) – HYGOV considered. CTCL6 (B) – HYGOV considered with Kundur optimum parameters. CTCL6 (C) – HYGOV not considered. 40

Figure 5.5 – Mechanical power response of the Caldeirão Unit 5 and the Furnas Unit 1 for the Pico Vermelho contingency. GCHRF (A) and G5CTCL (A) – HYGOV considered. GCHRF (B) and G5CTCL (B) – HYGOV not considered. 41

Figure 5.6 – Frequency response on the 60kV bus of the Caldeirão power plant for the Pico Vermelho contingency considering load shedding off. CTCL6 (A) – HYGOV considered. CTCL6 (B) – HYGOV considered with Kundur optimum parameters. CTCL6 (C) – HYGOV not considered. 42

Figure 5.7 – Frequency response on the 60kV bus of the Caldeirão power plant for the Pico Vermelho contingency. CTCL6 (A) – Hydro unit with $TM = 2,87$ and load shedding ON. CTCL6 (B) – Hydro unit with $TM = 12$ and load shedding ON. CTCL6 (C) – Hydro unit with $TM = 2,87$ and load shedding OFF. CTCL6 (D) – Hydro unit with $TM = 12$ and load shedding OFF. 43

Figure 5.8 – Frequency response on the 60kV bus of the Caldeirão power plant for the Caldeirão Unit 5 contingency. CTCL6 (A) – HYGOV considered. CTCL6 (B) – HYGOV considered with Kundur optimum parameters. CTCL6 (C) – HYGOV not considered. 44

Figure 5.9 – Mechanical power responses of the Furnas Unit 1 for the Caldeirão Unit 5 fault. GCHRF (A) – Hydro governor with trial and error optimum parameters. GCHRF (B) – Hydro governor with Kundur optimum parameters. GCHRF (C) – Hydro governor not considered. 45

Figure 5.10 – Frequency response on the 60kV bus of the Caldeirão power plant for the Caldeirão Unit 6 transformer contingency. CTCL6 (A) – HYGOV considered with load shedding ON. CTCL6 (B) – HYGOV considered with Kundur optimum parameters and load shedding ON. CTCL6 (C) – HYGOV considered with load shedding OFF. CTCL6 (D) - HYGOV considered with Kundur optimum parameters and load shedding OFF. 46

Figure 5.11 – Mechanical power responses of the Caldeirão Unit 3, the Furnas Unit 1 and the Caldeirão Unit 5 for the Caldeirão Unit 6 transformer contingency. Load shedding on. 47

Figure 5.12 – Mechanical power responses of the Caldeirão Unit 3, the Furnas Unit 1 and the Caldeirão Unit 5 for the Caldeirão Unit 6 transformer contingency. Load shedding off. 47

Figure 5.13 – Frequency response on the 60kV bus of the Caldeirão power plant for the Pico Vermelho contingency. CTCL6 (A) – HYGOV modelling a Francis turbine. CTCL6 (B) – HYGOV modelling a Pelton turbine. Load shedding is off. 48

Index of Tables

Table 3.1 – Generation profile for Summer Peak case.....	16
Table 3.2 – Voltage profile for 60 kV buses, SP case.....	17
Table 3.3 – Voltage profile for 30 kV buses, SP case.....	17
Table 3.4 – Voltage profile for 11 kV buses, SP case.....	17
Table 3.5 – Voltage profile for 10 kV buses, SP case.....	17
Table 3.6 – Voltage profile for 6,3 kV buses, SP case.....	17
Table 3.7 – Voltage profile for 0,4 kV buses, SP case.....	17
Table 3.8 – Generation profile for Winter Valley case.....	18
Table 3.9 – Voltage profile for 60 kV buses, WV case.....	18
Table 3.10 – Voltage profile for 30 kV buses, WV case.....	18
Table 3.11 – Voltage profile for 11 kV buses, WV case.....	18
Table 3.12 – Voltage profile for 10 kV buses, WV case.....	19
Table 3.13 – Voltage profile for 6,3 kV buses, WV case.....	19
Table 3.14 – Voltage profile for 0,4 kV buses, WV case.....	19
Table 3.15 – Synchronous generators parameters.....	20
Table 3.16 – Frequency relay regulation for Furnas induction motors.....	21
Table 3.17 – Under frequency regulation for loads.....	22
Table 4.1 – Base governor parameters.....	24
Table 4.2 – Effect of governor parameters for a unit with $TW = 2,0$ and $TM = 6,0$	24
Table 4.3 – Fixed HYGOV parameters.....	29
Table 4.4 – Optimum parameters choices for several units.....	31
Table 5.1 – Foros 60kV/30kV transformer contingency initial conditions.....	36
Table 5.2 – Pico Vermelho summer peak contingency, initial conditions.....	37
Table 5.3 – Load relay operations for Pico Vermelho summer peak contingency.....	39
Table 5.4 – Pico Vermelho winter valley contingency, initial conditions.....	39
Table 5.5 – Load relay operations for Pico Vermelho winter valley contingency.....	40
Table 5.6 – Caldeirão Unit 5 contingency initial conditions.....	43
Table 5.7 – Load relay operations for Caldeirão Unit 5 contingency.....	44
Table 5.8 – Caldeirão Unit 6 transformer contingency initial conditions.....	45
Table 5.9 – Load relay operations for Caldeirão Unit 6 transformer contingency.....	46
Table 5.10 – Initial conditions for the hydro turbine comparison case.....	48

List of Symbols

L	Penstock Length [m]
H	Head level [m]
A	Penstock cross-section area [m ²]
Q and q	Water flow [m ³ /s]
q_{base}	Rated turbine flow rate [m ³ /s]
q_{nl}	No load flow rate [m ³ /s]
q_r	Water flow at rated load [m ³ /s]
h_l	Head losses [m]
f_p	Head loss coefficient
h_0	Static head [m]
h_{base}	Rated head value [m]
h_r	Head at rated flow [m]
a_g	Gravity acceleration [m/s ²]
G and g	Real gate position
G_{min}	Minimum gate limit
G_{max}	Maximum gate limit
VELM	Gate velocity limit
T_W	Penstock water starting time [s]
P_M and P_{Mech}	Mechanical power [MW]
D_{turb}	Turbine damping coefficient
A_t	Turbine gain coefficient
Δw	Frequency or speed deviation [rad/s]
w_s	Synchronous speed reference [rad/s]
w_r	Machine rotor speed [rad/s]
Δg	Gate position deviation
ΔP_M	Mechanical power deviation [MW]
R_P	Permanent speed droop
R_T and r	Transient speed droop

T_R and T_r	Dashpot reset time [s]
T_P and T_f	Pilot valve time constant [s]
T_G	Gate servo motor time constant [s]
T_M	Mechanical starting time [s]
K_D	Load damping coefficient
T'_{d0}, T'_{q0}	d-axis and q-axis transient open circuit time constant [s]
T''_{d0}, T''_{q0}	d-axis and q-axis subtransient open circuit time constant [s]
H	Inertia time constant [s]
D	Speed damping
x_d, x'_d, x''_d	d-axis synchronous, transient and subtransient reactances
x_q, x'_q, x''_q	q-axis synchronous, transient and subtransient reactances
x_l	Stator leakage reactance

Chapter 1 - Introduction

1.1 Context and Motivation

Power systems are prone to suffer from disturbances, which may lead to wide excursions of its variables and cause equipment damage. Disturbances may be either small or large depending on their strength. The former occur as continuous small load changes in the system and can usually be interpreted as a small-signal stability problem. The latter are related to events of a severe nature, such as transmission line short-circuit, the tripping of a generator or a high amount of load and fall in the category of the transient stability problem. The larger a power system, the stronger and more resilient it is with respect to the effects of large disturbances, which cause the most significant excursions of system variables [1].

Controllers are used to contribute to the safe operation of the power system by maintaining system voltages, frequency, and other system variables within acceptable limits. Regulation of frequency is closely related to active power control while voltage regulation is closely related to reactive power control. These two regulation solutions can therefore be treated separately for a large class of problems [1].

Maintaining system frequency nearly constant ensures that the speed of induction and synchronous motors does not oscillate in an uncontrolled manner. A constant speed of motor drives is particularly important for a satisfactory performance of generating units as they are highly dependent on the behaviour of all the auxiliary drives, which are associated with the fuel, the feed water and the combustion air supply systems [1].

As has been noted before, system frequency and active power balance are tied together. This implies that a change in active power demand at one point in the network is propagated throughout the system as a change in frequency. The availability of many generators supplying power, distributed throughout the system, implies that a means to allocate power demand change to the generators should be provided. A controller denominated speed governor is usually installed on each generating unit. It has the capability to control the unit's mechanical power and the system frequency, a function commonly labelled as load-frequency control or primary frequency control. A unit's mechanical power is regulated by acting on the amount of resource available for energy transformation [1].

The main resources used for electrical energy generation are the kinetic energy of water and the thermal energy extracted from fossil fuels or nuclear fission. The generating unit, or prime mover, converts one resource into mechanical energy which is then converted to electrical energy by synchronous generators [1]. The usual practice is to resort to thermal power plants for the system frequency control duty to the detriment of the hydroelectric plants. The explanation resides in the inner nature of the process of energy conversion happening in each power plant. While for thermal power plants the principle of operation is the heated and high pressure steam which is converted into rotating energy in a steam turbine, in hydroelectric power plants mechanical motion is caused by the kinetic energy of water fed from the dam through a penstock. Naturally, the time constants of the processes

associated with energy conversion in thermal power plants are slightly smaller than those of a hydroelectric plant.

Nevertheless, in some cases, such as weaker or isolated power grids, hydroelectric power plants exhibit a significant contribution to system frequency regulation [2]. The study of the impact that changing speed governor parameters of hydroelectric power plants has on primary frequency regulation in an isolated grid is the scope of this work. A comparison with thermal power plants performance complements the analysis.

1.2 Objectives

In the context described above, the main objectives of this thesis are to illustrate the nature of the hydroelectric power plants speed governors in primary frequency control and to establish relationships between governor parameters and its hydro unit characteristic values. Finally, transient stability simulations are performed in an isolated grid with a high share of wind power, in order to observe to what degree hydroelectric power plants are capable of contributing to frequency regulation.

1.3 Thesis Outline

The thesis is organized in six chapters, including this introductory one, and one appendix.

Chapter 2 starts by providing a general picture of hydroelectricity. Modelling of the water turbine and water conduit system is presented, without considering the travelling wave phenomenon. Linear and nonlinear models for speed governors of hydroelectric power plants relevant to this work finalize this chapter.

Chapter 3 is dedicated to the description of the isolated grid, which is used to perform transient stability simulations.

Chapter 4 begins with the study of a linear hydroelectric speed governor in isolated operation, which serves as a guide to understand parameter influence in frequency oscillations. The second part of chapter 4 is devoted to trial and error optimization of a nonlinear hydroelectric speed governor model also in isolated operation.

Chapter 5 presents the results of dynamic simulations on the case study grid. Several contingencies are simulated, while the impact in frequency regulation of the hydroelectric speed governors is inspected and compared to the performance of the thermal units.

Chapter 6 finalizes by presenting conclusions and possible topics for future work.

Chapter 2 - Hydraulic Turbines and Governing Systems

2.1 Generalities

Four basic elements constitute hydraulic power plants, which are indispensable for the process of energy conversion from water: a way of creating a head level (a forebay), a penstock to convey water, a hydraulic turbine and an electric generator. These essential elements are depicted in Figure 2.1, followed by a brief description of each.

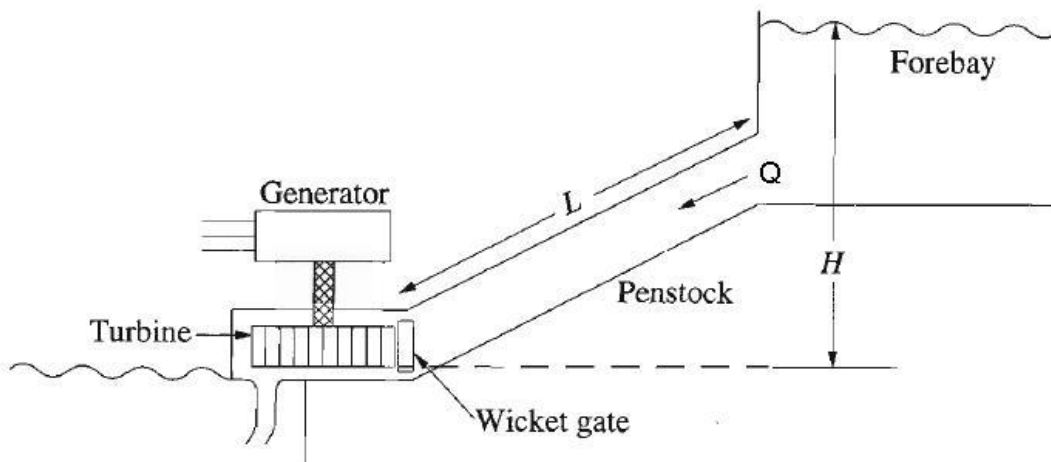


Figure 2.1 – Schematic of a hydroelectric power plant [1].

- The forebay, also usually denoted as reservoir, headrace or head pond, establishes the amount of water available for power production, impounding the water supply necessary for daily or seasonal stream flow release pattern into a large pipe, to the turbine. In some constructions one section of this pipe, called a conduit, is used to move the water to a point where a steep descent begins through the penstock to the turbine.
- A water column comprises all the structures used to direct the water from the head pond to the turbine. It may include an intake structure, the penstock and one or more surge tanks. Aspects like water column inertia, water compressibility and structure elasticity have an impact on the behaviour of the hydraulic turbine.
- The turbine is responsible for converting the water's kinetic energy into rotating mechanical energy, which in turn drives the generator. The amount of power produced is dependent on the available head at the turbine, its efficiency, and the flow rate of water admitted through the wicket gate. This wicket gate or water admission valve is placed in the terminal part of the penstock immediately before the turbine, and directly controls the amount of water flowing into the turbine.
- The generator takes part in the last energy conversion mechanism, extracting electrical energy from mechanical energy, synchronous generators being the elected choice. Induction motors

can be used for pumping water back to the reservoir if it is intended for the hydroelectric plant to include this option. Generator types and models are not exposed in detail, since it is out of the scope of this Thesis.

Hydraulic turbines, one of the elements of a hydroelectric plant, fall essentially into two major categories: impulse and reaction turbines. The former, commonly known as Pelton wheel, has a runner at atmospheric pressure with numerous spoon-shaped buckets mounted on its edge, which are driven by forceful streams of water issuing from nozzles. These high kinetic energy water jets that strike the buckets are subjected to a drop of momentum, providing the necessary torque to drive the runner. This type of turbine is used in hydro power plants with heads ranging from 15 to 1900 meters, although attaining higher efficiency for heads larger than 300 meters.

The latter, reaction turbines, operate under the principle that water flow takes place in a closed conduit system passing through stationary radial guide vanes and gates around the runner's periphery. Two subcategories exist: Francis and Kaplan. In the first, water flows impacting on the runner tangentially and exiting axially, being commonly used for heads up to 360 meters. The Kaplan turbine uses propeller-type wheels with adjustable blades. It is known for being an axial flow type of turbine since water flows parallel to the shaft and it's the common choice for heads less than 70 meters. Propeller turbines are a variant of the Kaplan type, with non-adjustable vanes, therefore being cheaper, simpler and requiring less maintenance. Pelton and Francis turbines are depicted in Figure 2.2 and Figure 2.3.

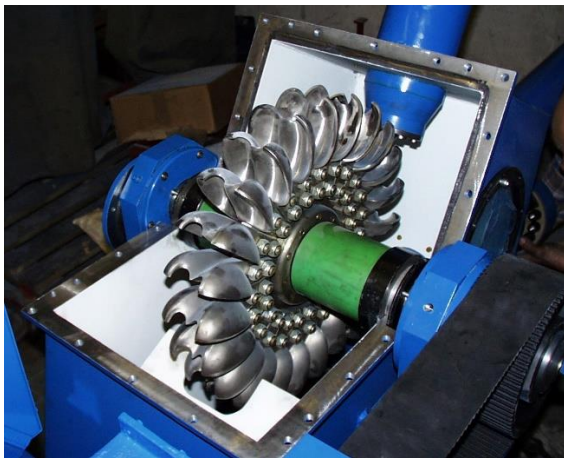


Figure 2.2 – Pelton Turbine.



Figure 2.3 – Francis turbine.

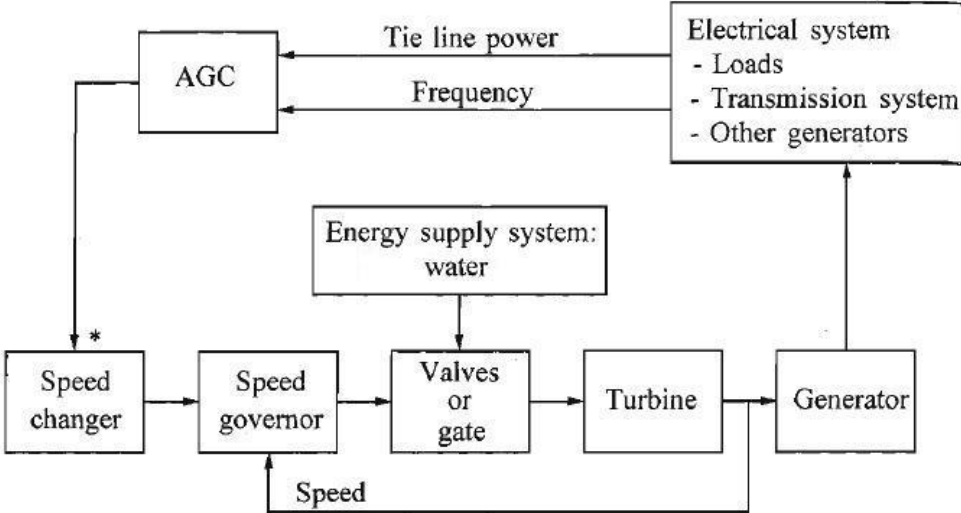
As mentioned earlier, the performance of a hydraulic turbine is influenced by the characteristics of the water column feeding the turbine, namely, the effects of water inertia, water compressibility and pipe wall elasticity in the penstock. Water inertia effect causes changes in turbine flow to lag behind changes in turbine gate opening or closing. The effect of pipe wall elasticity gives rise to travelling waves of pressure and flow in the conduits, a phenomenon commonly known as the “water hammer” [1]. Water hammer is defined as the occurrence of pressure fluctuations, caused when the system undergoes a change from one operational steady-state condition to another, that is, upon a change in the rate of water flow following a gate closing or opening. Pressure waves consequently travel along the penstock, subjecting pipe walls to great stresses. The classical solution to this water hammer problem is to insert

a device called a surge tank, a large tank that is usually located between the conduit and the penstock, in which water flows, converting kinetic energy to potential energy [2].

2.2 Modelling

Turbine-governor models are designed to give representations of the effects of hydroelectric power plants on power system stability. Accurate mathematical modelling of the hydraulic components includes the dynamic representation of penstock, surge tank if existent and the hydraulic losses of those elements. A functional diagram of the representation of a hydro turbine and its speed governor within the power system environment is portrayed in Figure 2.4.

Electric system performance, evaluated by measuring certain variables like voltages, power and frequency, is affected by the action of generators, network conditions and load behaviour. The hydro system, or prime mover, relates with the electrical system through mechanical power, which affects generator rotor speed and angle. The prime mover energy supply system responds to commands for generation variations, from speed deviations (primary speed control) and secondary speed control or AGC (automatic generation control) [2]. Frequency control mechanisms ensure the constancy of speed of generators, which is reflected in the balance between production and consumption of active power. This means that a change in power demand causes a frequency deviation, causing governor control systems to ensure that the machine follows up the demand change.



* AGC applied only to selected units

Figure 2.4 – Functional block diagram of hydraulic turbine generating system [1].

In the following sections, hydraulic turbine models and speed governing system models, which compose the prime mover, are presented.

2.2.1 Hydraulic Turbines

Transient characteristics of hydro turbines are determined by the dynamics of water flow in the penstock. Conversion of flow and head to power by the turbine involves non-dynamic relationships [3].

Precise modelling of hydraulic turbines requires that transmission-like wave effects, which take place in the elastic-walled pipes conducting the compressible fluid, are included. It has been observed that the speed of propagation of said travelling waves is approximately equal to the speed of sound in water, which is 1497 meters per second. Consequently, nonlinear travelling wave models are especially important for hydro power plants with long penstocks, which is not the case in the hydro site study demonstrated in this Thesis [1].

Although travelling wave models will not be addressed, in what follows, a nonlinear model is described, as it is more appropriate for large signal time domain simulations or transient stability studies. A block diagram for dynamic simulations of a hydraulic turbine with penstock, assuming unrestricted head and tailrace and without surge tank is shown in Figure 2.5. The penstock is modelled assuming an incompressible fluid and rigid conduit of length L and cross-section A . Penstock head losses h_f are proportional to flow squared and f_P is the head loss coefficient, usually ignored [4].

Pertaining to the laws of momentum, the rate of change of flow in the conduit is given by [4]

$$\frac{dq}{dt} = (h_0 - h - h_f) a_g \frac{A}{L} \quad (2.1)$$

where

q = turbine flow rate, in m³/sec

A = penstock cross-section area, in m²

L = penstock length, in m

a_g = acceleration due to gravity, in m/sec²

h_0 = static head of water column above turbine, in m

h = head at the turbine admission, in m

h_f = head loss due to friction in the conduit, in m.

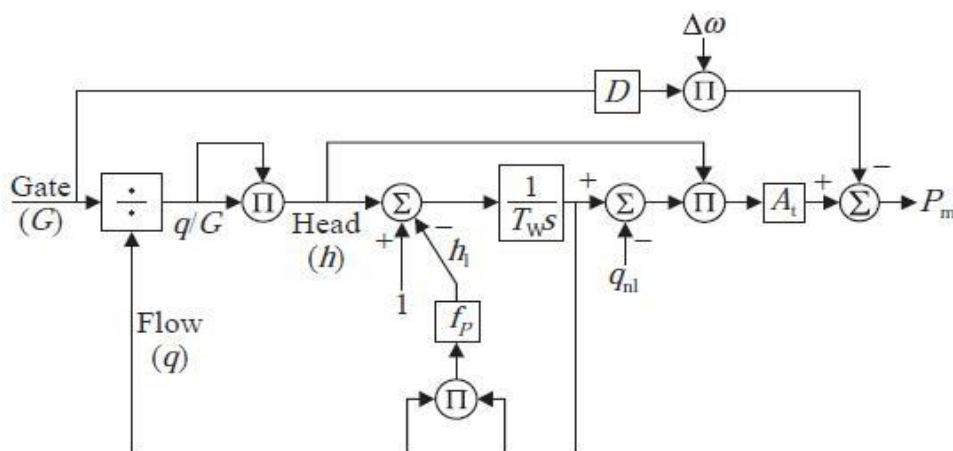


Figure 2.5 – Hydraulic turbine nonlinear model assuming inelastic water column [4].

Taking h_0 as the base head value h_{base} , which is equal to reservoir head minus the tailrace head, and setting q_{base} as the turbine flow rate with gates fully open, real gate position \bar{g} equal to 1 pu, expression (2.1) in per unit yields

$$\frac{d\bar{q}}{dt} = \frac{(1 - \bar{h} - \bar{h}_l)}{T_W} \quad (2.2)$$

where variables with superbars are per unit ones. The term T_W , given in seconds, is called the water time constant or water starting time in the penstock and represents the time required for a head h_{base} to accelerate the water in the penstock from standstill to the flow rate q_{base} . It is written as

$$T_W = \left(\frac{L}{A}\right) \frac{q_{base}}{h_{base} \cdot a_g} \quad (2.3)$$

From here on, the penstock head losses h_l are not taken into consideration. Turbine characteristics define base flow as a function of head and real gate position, $q = f(\text{gate}, \text{head})$, which is expressed in per unit as

$$\bar{q} = \bar{g}\sqrt{\bar{h}} \quad (2.4)$$

Mechanical power available from an ideal hydraulic turbine is the product of hydraulic head available and water flow rate, multiplied by appropriate conversion factors. Real turbine efficiency is not 100%, a fact that is accounted for by subtracting the no load flow, that weights the turbine fixed no load power losses, from the net flow giving the difference as the effective flow. A term representing the speed deviation damping effect is also to be included, which is a function of gate position. The per unit turbine mechanical power P_m , on generator MVA base, is thus expressed as

$$\bar{P}_m = A_t \bar{h} (\bar{q} - \bar{q}_{nl}) - D_{turb} \bar{g} \Delta \bar{\omega} \quad (2.5)$$

In the above formula, \bar{q}_{nl} corresponds to the per unit no load flow, D_{turb} , the turbine damping coefficient typically takes values in the range of 0,5 to 2,0 and A_t is a proportionality factor assumed constant, calculated using turbine MW rating and generator MVA base

$$A_t = \frac{1}{\bar{h}_r (\bar{q}_r - \bar{q}_{nl})} \frac{\text{Turbine MW rating}}{\text{Generator MVA rating}} \quad (2.6)$$

where \bar{h}_r is defined as the per unit head at rated flow (usually 1 pu) and \bar{q}_r is the per unit flow at rated load.

An important remark about this parameter is that in some stability programs, parameter A_t , also called turbine gain, is used to convert the real gate position to the ideal gate position, that is, $A_t = 1/(\bar{g}_{FL} - \bar{g}_{NL})$. This ratio is explicit in Figure 2.6. A separate factor is then applied to convert the power from the turbine rated power base to that of the generator volt-ampere base. This is not the case of PSS/E, where models consider A_t as defined (2.6).

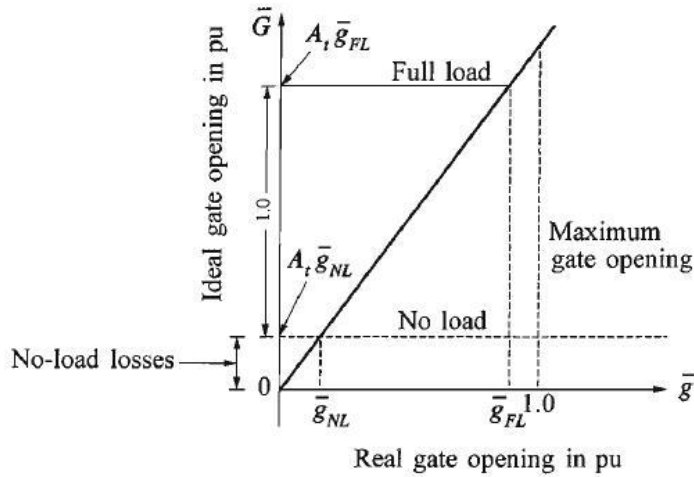


Figure 2.6 – Relationship between ideal and real gate positions [1].

Having presented the nonlinear model, the rest of this section will be devoted to describe the linear model. Realizing that linear models are developed by linearization around an operating point, they are also designated as small-signal models.

Linearizing the basic penstock and turbine relationships, (2.4) and (2.2) as presented in the nonlinear model, and neglecting friction losses, Figure 2.5 simplifies to the block diagram in Figure 2.7.

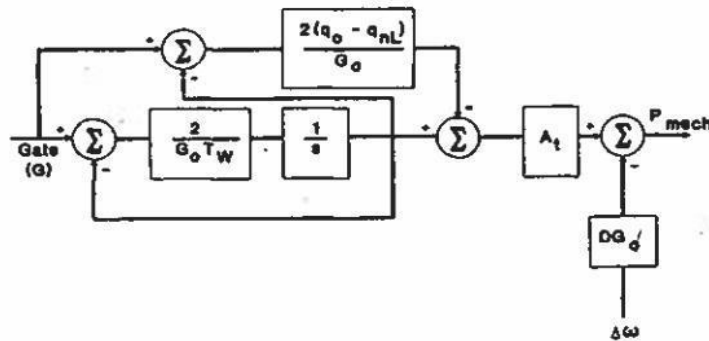


Figure 2.7 – Linear turbine model with inelastic water column [4].

As can be inferred from Figure 2.7, change in mechanical power output in terms of gate position, speed deviation and constructive parameters is expressed as [4]

$$\Delta \bar{P}_m = \frac{A_t(1 - T_1 s)\Delta \bar{g}}{(1 + T_2 s)} - D \bar{g}_0 \Delta \bar{\omega} \quad (2.7)$$

where

\bar{g}_0 = per unit real gate opening at operating point.

$T_1 = (\bar{q}_0 - \bar{q}_{nl})T_w$, in s.

$T_2 = \bar{g}_0 T_w / 2$, in s.

\bar{q}_0 = per unit steady state flow rate at operating point.

Note that $\bar{q}_0 = \bar{g}_0$ in equation (2.7). If the damping term D is neglected a similar expression to the usual classical turbine-penstock transfer function is achieved

$$\frac{\Delta \bar{P}_m}{\Delta \bar{g}} = \frac{1 - \bar{g}_0 T_w s}{1 + \frac{\bar{g}_0 T_w s}{2}} A_t \quad (2.8)$$

where the term $\bar{g}_0 T_w$ can be seen as an approximation to the effective water starting time constant for small perturbations around a specific operating point. This means that, contrary to the nonlinear model where T_w is determined using rated values of head and flow, therefore making it a fixed value, when using the linear model the effective water starting time corresponds to the chosen operating condition and needs to be adjusted each time that operating condition is modified.

Transfer function (2.8) has the special characteristic of representing a non-minimum phase system, which can be shown by determining its time response to a change in gate position, given by [1]

$$\Delta \bar{P}_m(t) = [1 - 3e^{-\frac{2t}{T_w}}] \Delta \bar{g} \quad (2.9)$$

where \bar{g}_0 was assumed to be equal to 1 pu. Taking $T_w = 4$ as an example, the previous time response is plotted in Figure 2.8, following a unit step increase in gate position.

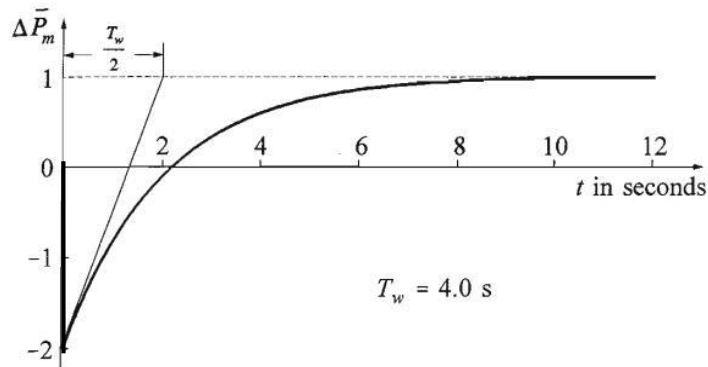


Figure 2.8 – Turbine power change due to a unit step gate opening [1].

It is readily observed that mechanical power starts by decreasing by 2 pu, contrary to the increment of gate position. Water inertia causes this initial surge because upon the sudden gate opening, flow does not change immediately. Despite that fact, pressure across the turbine is reduced, leading to a reduction in power. For $t > 0$, the increase is exponential with a $T_w/2$ time constant reaching a steady state value of 1 pu above the initial operating point.

2.2.2 Speed Governors

The governing system is responsible for assuring turbine-governor primary speed regulation and therefore frequency and active power, upon detecting load variations. The control mechanism includes equipment such as relays, servomotors, pressure or power amplifying devices, levers and linkages. The speed governor normally actuates on the governor controlled gates which in turn regulates the water inlet to the turbine. Figure 2.9 depicts the general hydraulic governing system.

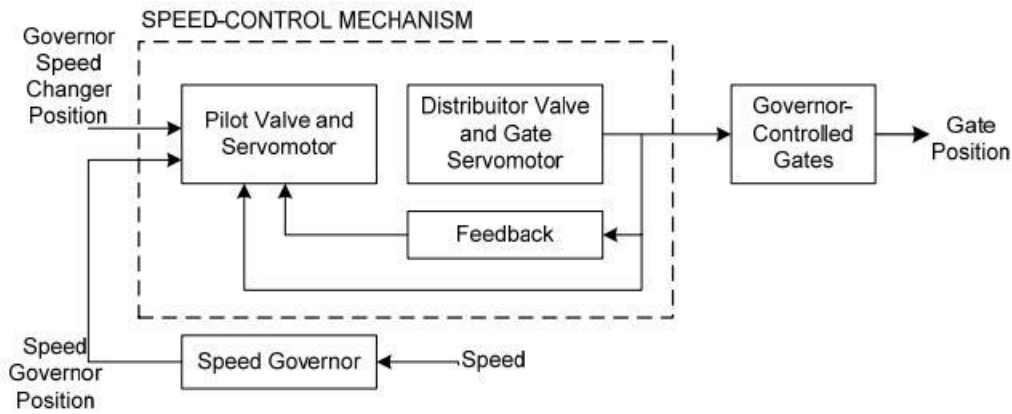


Figure 2.9 – Hydraulic plant governing system schematic [3].

The primary speed control function consists on feeding back the speed error to control gate position. The controller compares the speed measured in the prime mover with the reference speed (set point input). The resulting error from this comparison is a signal that the governor uses to command the actuator, which in turn acts on the control device, operating the gate position. Since the goal is to ensure satisfactory and stable parallel operation of multiple generating units, speed controllers are provided with a droop characteristic, each. The purpose of this steady state droop is to make sure that load will be equally shared between all units, otherwise they would compete with each other trying to control system frequency to its own setting. For each unit, it determines the amount of change in output that the unit produces in response to a change in speed. A typical value for the permanent speed droop is 5%, which means that, assuming the generator is supplying an isolated load, a speed deviation of 5% causes a 100% change in power output [1]. Figure 2.10 illustrates this attribute.

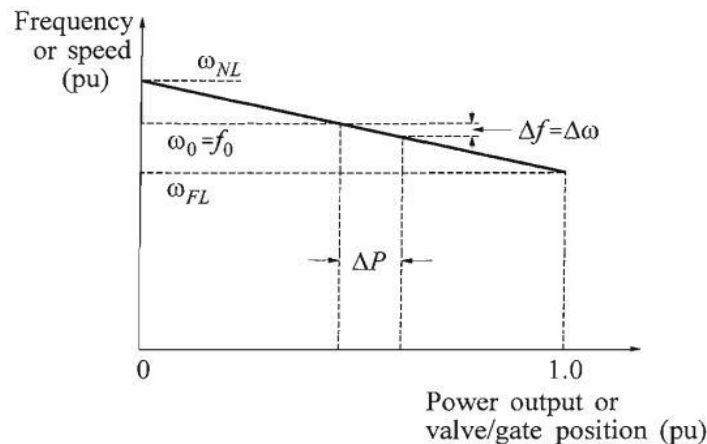


Figure 2.10 – Ideal steady state characteristic of governor with speed droop [1].

This last setting by itself however, is not enough for the role of ensuring stability operation of the unit. As was shown with Figure 2.8, the water inertia effect causes the hydro turbine response to be one of a non-minimum phase system, that is, a gate change originates an initial power change opposite to that intended. Two direct consequences arise from this fact, the first one being the need to employ the use of two servomotors to provide the required force to move the control gate. The pilot servomotor, low

powered, operates the distributor or relay valve of the main gate servomotor, which is the high power one. Connected to the pilot servomotor, a pilot valve is commanded either by a mechanical governor or an electronic regulator.

The second consequence, which complements the speed droop setting in assuring stability of the unit, is the requirement for a large transient droop with a relatively long resetting time. This requirement is met by feeding back real gate position into a transient gain reduction compensator as show in Figure 2.12. In this fashion, gate movement will be limited or delayed, in order to allow for water flow to catch up and therefore the power delivered by the turbine. This delay on gate position movement depends on the reset time T_R , during which, the effect of temporary droop prevails over the permanent droop, leaving the latter to determine the steady state response of the unit. Evidently, the governor will exhibit high droop setting R_T , hence low gain during transient condition, and the aforementioned permanent droop R_p or high gain in steady state mode [1].

The first speed governing systems were realizable using the Watt centrifugal mechanism, composed of mechanical and hydraulic components. Speed measuring, permanent droop compensation and computing functions are doable resorting to mechanical components, while hydraulic components are responsible for functions requiring high power. Transient droop compensation is provided by a dashpot that can be enabled or disabled if a bypass arrangement is included [1]. A simplified illustration of a mechanical-hydraulic governor is shown in Figure 2.11.

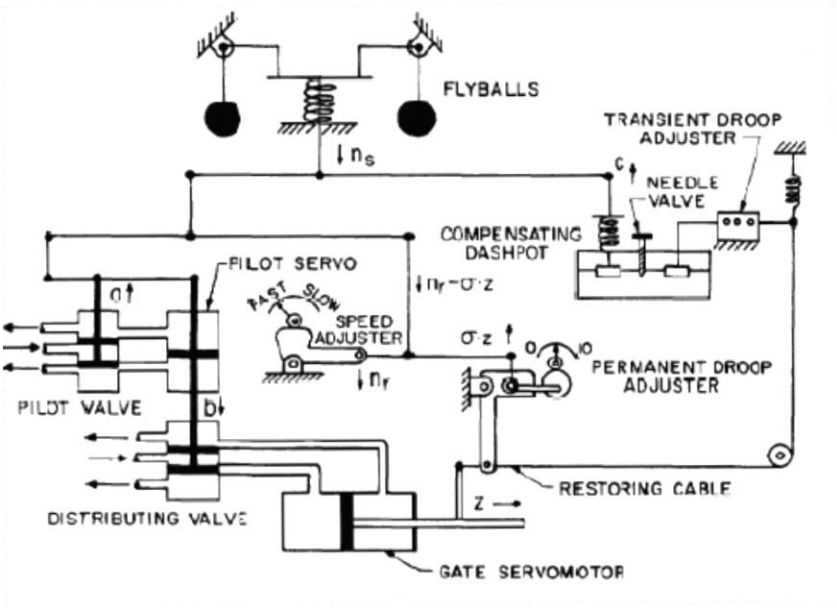


Figure 2.11 - Mechanical-Hydraulic governor for hydro turbine [5].

In steady state machine rotor speed signal w_r (n_s in Figure 2.11) is compared with the reference speed w_s (n_r in Figure 2.11), and modified by the product of gate position \bar{g} (z in Figure 2.11) to the permanent speed droop R_p (σ in Figure 2.11). This difference is reflected as a change in the input a to the pilot servo. When gate position is changing, a transient droop signal c is generated in order to oppose sudden changes in gate position. These summed signals are then transmitted via a system of floating levers from a mechanical motion to the operation of the pilot valve [5].

Taking Figure 2.11 as a starting point, transfer function of the distributing valve and gate servomotor is [1]

$$\frac{\bar{g}}{b} = \frac{K_1}{s} \quad (2.10)$$

while pilot valve and pilot servo transfer function is

$$\frac{b}{a} = \frac{K_2}{1 + sT_p} \quad (2.11)$$

where K_2 is calculated by feedback lever ratio and T_p , the pilot valve time constant, by the pilot valve port areas and K_2 . The combination of (2.10) and (2.11) results in

$$\frac{\bar{g}}{a} = \frac{K_1 K_2}{s(1 + sT_p)} = \frac{K_S}{s(1 + sT_p)} \quad (2.12)$$

where K_S represents the servo gain, determined by pilot valve feedback lever ratio and the port areas of the distributing valve and gate servo.

The compensating dashpot in Figure 2.11 consists of a mechanical device, a damper that resists motion. As stated before, a bypass arrangement may be used in order to permit fast unrestricted motion in one direction and slow fluid motion using the dashpot in the opposite direction. Under the assumption that the dashpot fluid flowing through the needle is proportional to the dashpot pressure, the transfer function for the compensating dashpot is given by

$$\frac{c}{\bar{g}} = R_T \frac{sT_R}{1 + sT_R} \quad (2.13)$$

where temporary droop R_T is obtained by selection of pivot point for the lever connecting the input piston and reset time T_R by the needle valve setting.

Pilot valve input signal a is produced with a floating levers system, adding rotor speed, reference speed, permanent droop and temporary droop signals

$$a = \bar{w}_s - \bar{w}_r - R_P \bar{g} - R_T \frac{sT_R}{1 + sT_R} \quad (2.14)$$

The block diagram of Figure 2.12 represents the hydro governing system, with all signals given in per unit, inferred from the above transfer functions, which by association with the turbine model in Figure 2.5 provides a unified nonlinear model of hydro turbine and governing system. It should be noted that gate movement is rated limited (equal to the reciprocal of the time taken for the gates to move from fully open to fully closed position), a direct consequence of the fact that if the gate is closed too rapidly the resulting pressure may severely damage the penstock [1].

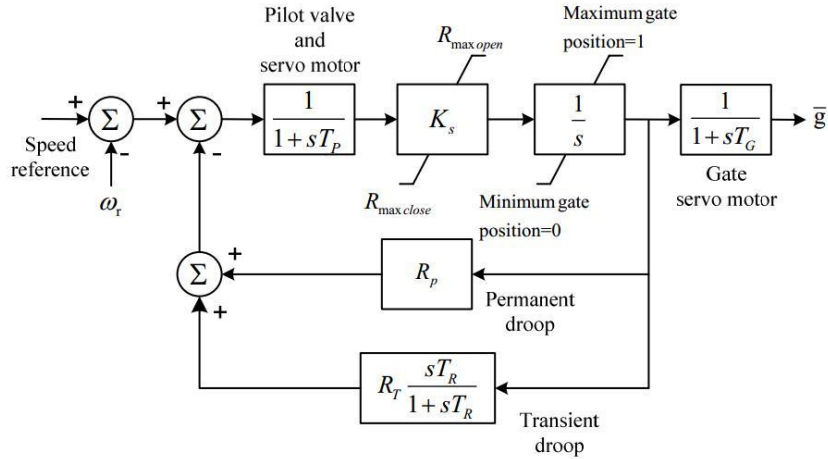


Figure 2.12 – Hydraulic turbine governor model [6].

If the above model is linearized, its combination with the linear turbine model from equation (2.8) results in the schematic of Figure 2.13. In this diagram $G_c(s)$ represents the transient droop compensation, T_p , usually being the lowest value time constant, is neglected and the generator is represented in terms of its inertia T_M and the load damping coefficient K_D .

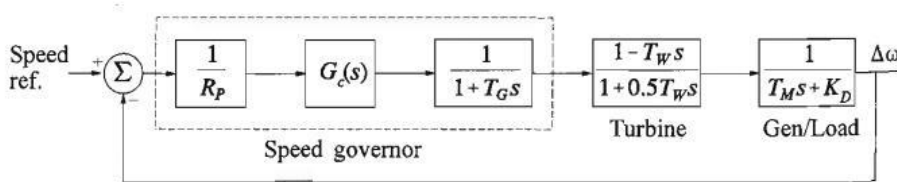


Figure 2.13 – Block diagram of linear governing system [1].

Since 1960 the usage of electro-hydraulic governors to the detriment of the conventional mechanical-hydraulic governors has prevailed, as the former are capable of providing greater flexibility and better performance. Both are functionally very similar, with speed sensing, droop compensation and computing functions being executed electrically, in the case of electro-hydraulic systems. Pilot valve and its servomotor are operated by means of an electrical-mechanical transducer signal driven [5]. When modelling the electric governor, its dynamic characteristics are often adjusted to be fundamentally similar to the mechanical-hydraulic governor ones, hence the previous model of Figure 2.12 applies [1].

Chapter 3 - Case Study Network

3.1 Network Composition

The São Miguel island grid, in Açores archipelago, is used as the case study in this work. It is operated with a rated frequency of 50 Hz, following the European standard. The grid, which is modelled and simulated with PSS/E, consists of 48 buses connected through 20 power lines and 45 transformers, 5 power generation sites, 3 fixed shunt compensators and 22 loads. One additional power generation site, the Furnas hydroelectric plant, is to be constructed in the near future, which means that the generation and load profiles used in the simulations are referred to the year 2020. Throughout the case study analysis two scenarios are considered, the summer peak (SP) corresponding to a 75,9 MW and 27,6 Mvar load profile and the winter valley (WV) corresponding to a 34,7 MW and 10,9 Mvar load profile. Regarding generation, the following list gives a brief description of each power plant.

- Caldeirão thermal power plant (CTCL), consists of 4 groups of 9,62 MVA and another 4 groups of 21,28 MVA.
- Ribeira Grande geothermal power plant (CGRG), has 2 groups of 3,625 MVA and 2 groups of 6,75 MVA.
- Pico Vermelho geothermal power plant (CGPV), with 1 group of 16,25 MVA and 1 group of 6,25 MVA.
- A waste incineration plant (CVE), consisting on a single group of 9,8 MVA.
- Furnas hydroelectric power plant (CHRF), composed of 2 generation groups of 7,1375 MVA each and 4 groups of induction motors with a 3,51 MVA rate each, to be used in pumping water back to this plant's reservoir.
- Graminhais wind park (PEGR), with 10 wind turbines of 0,9 MW each.

All network components are modelled according to the information provided by the EDA utility (Electricidade dos Açores), responsible for grid commissioning. The grid schematic is pictured in Appendix A.

3.2 Power Flow Results

Several hypotheses have to be assumed in order to perform the power flow simulations for the two scenarios mentioned in the previous section, which are:

- Voltage in generation buses is set to 1 pu, except for the buses connecting Graminhais wind park and the waste incineration plant. In those cases power factor is taken to be equal to unity, meaning these power plants do not exchange reactive power with the network.
- Taps of the transformers belonging to the Caldeirão power plant are adjusted so that its 60 kV bus voltage takes a value between 1,035 pu and 1,045 pu, corresponding to the voltage range [62,1 kV – 62,7 kV].
- Shunt compensation in Aeoroporto substation (SEAE) is connected to the grid in the Summer Peak scenario and disconnected in the Winter Valley scenario. Shunt compensation installed in Ponta Delgada substation (SEPD) remains connected in both scenarios.

- It is assumed that the reactive power consumed by the induction motors in Furnas hydroelectric plant is compensated by the generation units of the power plant. These motors only operate in the Winter Valley scenario, where the generation units are set to run as synchronous compensators, hence not transferring active power to the network.

The Newton-Raphson method is the elected option for computing the power flow solutions.

3.2.1 Summer Peak

The load profile for the Summer Peak case, as stated in section 3.1, is equal to 75,9 MW and 27,6 Mvar. In this context, the dispatch of the power plants in service for this scenario is as follows:

- Graminhais wind park is set to 30% of its installed capacity. The basis behind this value was a study of the wind distribution during the summer in São Miguel.
- Both geothermal power plants (Pico Vermelho and Ribeira Grande) are set to their rated capacity, totalling 29 MW.
- Waste incineration plant is dispatched to generate 6,7 MW.
- The two generation units in the Furnas hydroelectric plant are set to operate at their full capacity, injecting a total of 11,42 MW. As previously mentioned the induction motors are not in operation in this scenario.
- The generation balance is closed by the Caldeirão power plant, with two units of higher rated power and one unit of lower rated power in service. The bus to which one of the higher rated power units is connected (specifically unit 5), is chosen to represent the swing bus.

The units dispatch followed by the power flow simulation lead to the production profile in Table 3.1.

Table 3.1 – Generation profile for Summer Peak case.

	Injected Active Power [MW]	Injected Reactive Power [Mvar]
Graminhais	2,73	0
Ribeira Grande	13,00	0
Pico Vermelho	16,00	0
Waste Incineration	6,70	0
Furnas	11,42	0,49
Caldeirão	27,27	27,43
Total	77,12	27,92

Total losses for this scenario are 1,18 MW, corresponding to 1,54% of total injected active power. The following tables present the results for the voltage magnitudes and angles of the different voltage rated sub-grids.

Table 3.2 – Voltage profile for 60 kV buses, SP case.

Bus ID	CTC L6	SEM F6	SEA E6	SEP D6	SES R6	SEL G6	SEP G6	SEF O6	CGR G6	CGP V6	PEG R6	SEC L6	CHR F6
Voltage [pu]	1,039	1,035	1,036	1,034	1,036	1,039	1,043	1,041	1,045	1,043	1,045	1,039	1,046
Angle [°]	-1,63	-2,03	-2,07	-2,11	-1,87	-1,41	-0,42	-0,86	-0,25	-0,51	-0,22	-1,63	-0,08

Table 3.3 – Voltage profile for 30 kV buses, SP case.

Bus ID	G1CVE	SECL3	SEMF3	SEVF3	SEPG3	SELG3	PEGR3	SEFO3
Voltage [pu]	1,048	1,042	1,047	1,028	1,033	1,020	1,045	1,030
Angle [°]	-1,66	-1,78	-3,71	-1,5	-1,28	-2,39	0,68	-2,13

Table 3.4 – Voltage profile for 11 kV buses, SP case.

Bus ID	CGPV	G5CTCL	G6CTCL	G7CTCL	G8CTCL
Voltage [pu]	1,045	1,000	1,000	1,000	1,000
Angle [°]	2,41	0	1,11	0	0

Table 3.5 – Voltage profile for 10 kV buses, SP case.

Bus ID	CGRG	SEAE1	SEPD1	SESR1	SELG1	SEVF1	SEFO1
Voltage [pu]	1,048	1,033	1,025	1,027	1,027	1,025	1,033
Angle [°]	3,13	-3,59	-3,65	-2,95	-2,64	-1,83	-1,8

Table 3.6 – Voltage profile for 6,3 kV buses, SP case.

Bus ID	CHRF	G1CTCL	G2CTCL	G3CTCL	G4CTCL
Voltage [pu]	1	1	1	1	1
Angle [°]	2,65	0	0	0,74	0

Table 3.7 – Voltage profile for 0,4 kV buses, SP case.

Bus ID	G1PE GR	G2PE GR	G3PE GR	G4PE GR	G5PE GR	G6PE GR	G7PE GR	G8PE GR	G9PE GR	G10PE GR
Voltage [pu]	1,048	1,048	1,048	1,048	1,048	1,048	1,048	1,048	1,048	1,048
Angle [°]	1,5	1,5	1,5	1,5	1,5	1,5	1,5	1,5	1,5	1,5

As is readily observed from the voltage profiles, all voltage magnitude values fall in the range of 0,95 pu to 1,05 pu, which means that the power flow solution is acceptable, else different transformer taps settings would have to be experimented. Due to the relatively high amount of branches in this grid, the power flowing in each of them is not presented here, but the analysis of those values as listed by PSS/E reflects that no overcharging limits are infringed.

3.2.2 Winter Valley

The load profile for the Winter Valley case, as indicated in section 3.1, is equal to 34,7 MW and 10,9 Mvar. For this scenario the power plants dispatch is defined by the following points:

- Graminhais wind park is again set to 30% of its installed capacity. The basis behind this value was a study of the wind distribution during the winter in São Miguel.
- Both geothermal power plants (Pico Vermelho and Ribeira Grande) are set to their rated capacity, totalling 29 MW.
- Waste incineration plant is dispatched to generate 3,8 MW.
- In this scenario 4 units consisting of induction motors operating pumps, in Furnas hydro plant, are dispatched to absorb 2,5 MW each, totalling 10 MW. The 2 generation units are operated as synchronous compensators, therefore not injecting any active power to the system.
- As in the Summer Peak scenario, Caldeirão power plant closes the generation balance, with only one higher rated power unit allocated to the dispatch.

The units dispatch followed by the power flow simulation lead to the production profile in Table 3.8.

Table 3.8 – Generation profile for Winter Valley case.

	Injected Active Power [MW]	Injected Reactive Power [Mvar]
Graminhais	2,73	0
Ribeira Grande	13,00	0
Pico Vermelho	16,00	0
Waste Incineration	3,80	0
Furnas	-10,00	3,89
Caldeirão	9,92	6,99
Total	35,45	10,89

Total losses for this scenario are 0,75 MW, corresponding to 2,11% of total injected active power. The following tables present the results for the voltage magnitudes and angles of the different voltage rated sub-grids.

Table 3.9 – Voltage profile for 60 kV buses, WV case.

Bus ID	CTC L6	SEM F6	SEA E6	SEP D6	SES R6	SEL G6	SEP G6	SEF O6	CGR G6	CGP V6	PEG R6	SEC L6	CHR F6
Voltage [pu]	1,038	1,037	1,037	1,037	1,037	1,038	1,037	1,040	1,044	1,042	1,039	1,038	1,037
Angle [°]	-1,95	-2,13	-2,15	-2,17	-2,07	-1,88	-2	-1,5	-1,01	-1,27	-1,79	-1,95	-2,35

Table 3.10 – Voltage profile for 30 kV buses, WV case.

Bus ID	G1CVE	SECL3	SEMF3	SEVF3	SEPG3	SELG3	PEGR3	SEFO3
Voltage [pu]	1,026	1,023	1,030	1,021	1,028	1,032	1,040	1,036
Angle [°]	-1,71	-1,78	-3,06	-2,64	-2,51	-2,39	-0,89	-2,26

Table 3.11 – Voltage profile for 11 kV buses, WV case.

Bus ID	CGPV	G5CTCL	G6CTCL	G7CTCL	G8CTCL
Voltage [pu]	1,044	1,000	1,000	1,000	1,000
Angle [°]	1,65	0	0	0	0

Table 3.12 – Voltage profile for 10 kV buses, WV case.

Bus ID	CGRG	SEAE1	SEPD1	SESR1	SELG1	SEVF1	SEFO1
Voltage [pu]	1,047	1,031	1,036	1,032	1,046	1,037	1,036
Angle [°]	2,38	-2,87	-2,73	-2,67	-2,22	-2,96	-2,01

Table 3.13 – Voltage profile for 6,3 kV buses, WV case.

Bus ID	CHRF	G1CTCL	G2CTCL	G3CTCL	G4CTCL
Voltage [pu]	1	1	1	1	1
Angle [°]	-4,83	0	0	0	0

Table 3.14 – Voltage profile for 0,4 kV buses, WV case.

Bus ID	G1PE GR	G2PE GR	G3PE GR	G4PE GR	G5PE GR	G6PE GR	G7PE GR	G8PE GR	G9PE GR	G10PE GR
Voltage [pu]	1,042	1,042	1,042	1,042	1,042	1,042	1,042	1,042	1,042	1,042
Angle [°]	-0,06	-0,06	-0,06	-0,06	-0,06	-0,06	-0,06	-0,06	-0,06	-0,06

By inspection of the tables above, voltage magnitude values fall in the range of 0,95 pu to 1,05 pu, which again, means that the power flow solution is acceptable. Due to the relatively high amount of branches in this grid, the power flowing in each of them is not presented here, but the analysis of those values as listed by PSS/E reflects that no overcharging limits are surpassed.

3.3 Dynamic Models

In order to study the impact of the Furnas hydroelectric plant on the grid operation it is necessary to employ the use of dynamic models, which give an image of the real behaviour of the systems equipping the several generation sites. They are as follows:

1) Generator Models

Data retrieved from EDA indicates that generators in Caldeirão thermal power plant are salient pole machines.

Concerning the geothermal plants of Ribeira Grande and Pico Vermelho, despite having a rated speed of 1500 rpm (2 pole machines), their direct and quadrature axis stationary reactances are very different, which justifies the choice of modelling these plants as salient pole machines.

The waste incineration plant is modelled as an equivalent thermal plant, thus a salient pole machine model is chosen.

Furnas hydroelectric power plant is assumed to be equipped with two Pelton turbines. Typically the generators driven by Pelton type turbines have 3 or 4 pole pairs, therefore are also modelled as salient pole machines. In addition to the two generation units the plant has 4 pump units, which are modelled as induction motors.

Finally, Graminhais wind park is equipped with machines provided by the manufacturer ENERCON. PSS/E, the software used in this work, contains in its library a module made available by ENERCON to

be used when modelling their wind turbines. Naturally, it was the model used. Pertaining to the salient pole generators the appropriate model in PSS/E's library is GENSAL. Magnetic saturation affects the various mutual and leakage inductances within the machine, a fact that is recognized by the GENSAL model. This model assumes that saturation affects only the direct axis and models it as a quadratic function. All the parameters assigned to the salient pole generators are shown in Table 3.15.

Table 3.15 – Synchronous generators parameters.

Bus ID	Model	ID	T'd0	T''d0	T''q0	H	D	xd	xq	x'd	x''d	xl	S(1,0)	S(1,2)
G1CTCL	GENSAL	1	5,8	0,07	0,28	1,96	0,01	2,3	1,32	0,43	0,215	0,1	0,28	0,95
G2CTCL	GENSAL	1	5,8	0,07	0,28	1,96	0,01	2,3	1,32	0,43	0,215	0,1	0,28	0,95
G3CTCL	GENSAL	1	5,8	0,07	0,28	1,96	0,01	2,3	1,32	0,43	0,215	0,1	0,28	0,95
G4CTCL	GENSAL	1	5,8	0,07	0,28	1,96	0,01	2,3	1,32	0,43	0,215	0,1	0,28	0,95
G5CTCL	GENSAL	1	5,9	0,033	0,132	4,46	0,01	1,86	0,93	0,31	0,207	0,1	0,14	0,41
G6CTCL	GENSAL	1	5,9	0,033	0,132	4,46	0,01	1,86	0,93	0,31	0,207	0,1	0,14	0,41
G7CTCL	GENSAL	1	5,9	0,033	0,132	4,46	0,01	1,86	0,93	0,31	0,207	0,1	0,14	0,41
G8CTCL	GENSAL	1	5,9	0,033	0,132	4,46	0,01	1,86	0,93	0,31	0,207	0,1	0,14	0,41
CGRG	GENSAL	1	5,593	0,056	0,0728	4,9	0,01	2,774	1,646	0,388	0,341	0,1	0,11	0,4
CGRG	GENSAL	2	5,593	0,056	0,0728	4,9	0,01	2,774	1,646	0,388	0,341	0,1	0,11	0,4
CGRG	GENSAL	3	8,045	0,08	0,104	1,6	0,01	2,16	1,17	0,329	0,265	0,1	0,11	0,4
CGRG	GENSAL	4	8,045	0,08	0,104	1,6	0,01	2,16	1,17	0,329	0,265	0,1	0,11	0,4
CGPV	GENSAL	1	6	0,06	0,08	0,64	0,5	2,15	1,09	0,29	0,19	0,1	0,11	0,4
CGPV	GENSAL	2	8,045	0,08	0,104	1,6	0,01	2,16	1,17	0,329	0,265	0,1	0,11	0,4
CVE	GENSAL	1	5,03	0,08	0,19	2,52	0,01	2,254	1,127	0,311	0,172	0,1	0,11	0,4
CHRF	GENSAL	1	3,8	0,015	0,077	1,43	0,01	1,52	1	0,2	0,13	0,1	0,11	0,4
CHRF	GENSAL	2	3,8	0,015	0,077	1,43	0,01	1,52	1	0,2	0,13	0,1	0,11	0,4

The parameters designation in the table above is the usual, except for $S(1,0)$ and $S(1,2)$ which define the magnetic saturation function, and x_l that represents the leakage reactance of the stator winding. T'_{d0} , T''_{d0} , T''_{q0} and H are given in seconds, while all other variables are expressed in pu.

2) Excitation System Models

The publication “*IEEE Recommended Practice for Excitation System Models for Power System Stability Studies*” issued by IEEE lists the models that are adequate to use for any given voltage regulator manufacturer. Models chosen for Caldeirão and the two geothermal plants are based on this publication.

According to EDA, Caldeirão power plant is equipped with Unitrol voltage regulators manufactured by ABB. The suggested model to use in PSS/E is the ST1A type, which represents a system where the excitation power is supplied through a transformer from the generator terminals and regulated by a controlled rectifier.

The geothermal power plants are equipped with KCR-760 voltage regulators manufactured by Kato, which represent a brushless excitation system where the power is supplied by a permanent magnet generator. The chosen model from the PSS/E library is the AC5A by IEEE.

For the waste incineration plant and the Furnas hydroelectric plant the elected model is the IEEE1, which is generally employed when excitation system details are unknown. It can represent systems with shunt dc exciters as well as systems with alternator exciters and uncontrolled shaft mounted rectifier bridges.

3) Speed Governor Models

Speed governor modelling is approached by first considering which power plants contribute to the primary frequency governing.

Information provided by EDA on the behaviour of the geothermal plants when a disturbance occurs in the system shows that these plants do not participate in primary frequency control, therefore maintaining their mechanical power constant. The same conclusion is taken for the waste incineration power plant.

Caldeirão thermal plant, which takes part in both primary and secondary frequency control, is equipped with diesel engines. The most adequate model for this type of units, in PSS/E's library, is the DEGOV1, which is based on a Woodward governor consisting of an electric speed sensor, a hydro-mechanical actuator and the diesel engine.

With regard to the hydroelectric power plant, a model suitable for the study of large speed perturbations in the power system is the HYGOV, for which the bases have been established in chapter 2. It represents a simple hydroelectric governor with a basic representation of the penstock, therefore not modelling travelling wave phenomena nor the effect of a surge tank. An in-depth study of this model is presented in chapter 4, as its impact on frequency regulation of the network is the scope of this work.

4) Load Models

Last but not least, models for the induction motors belonging to Furnas hydroelectric plant and frequency relay models for both the induction motors and for several loads of the system are used.

For the induction motors the chosen model is the CIMTR4, which may be used to represent either a single-cage or double-cage induction motor with rotor flux dynamics included. Frequency relay models are also applied to the motors, which cause their detachment from the network when bus frequency decreases/increases below/above a threshold value. The frequency relay model used is the FQRTPA and its parameterization for the induction motors is shown in Table 3.16.

Table 3.16 – Frequency relay regulation for Furnas induction motors.

Bus ID	ID	LFT [Hz]	UFT [Hz]	TP [s]	TB [s]
CHRF	3	49	55	0,02	0,08
CHRF	3	45	51,5	0,02	0,08
CHRF	4	49	55	0,02	0,08
CHRF	4	45	51,5	0,02	0,08
CHRF	5	49	55	0,02	0,08
CHRF	5	45	51,5	0,02	0,08
CHRF	6	49	55	0,02	0,08
CHRF	6	45	51,5	0,02	0,08

In the table above *LFT* represents the lower frequency threshold, *UFT* the upper frequency threshold, *TP* the relay pickup time and *TB* the breaker opening time.

Regarding the remaining 22 loads, dynamic load models are not used, instead, load components are expressed as algebraic functions of bus voltage magnitude prior to the dynamic simulation and remain constant through it. Active power is modelled with a constant current characteristic while reactive power is modelled with a constant admittance characteristic.

As mentioned before, frequency relays are also employed on loads, specifically under frequency ones. PSS/E provides specific models for this purpose and LDSHBL is the choice. Its operation principle is similar to the FRQTPA one, with the exception that LDSHBL has the option for multiple load shedding stages and does not operate with upper thresholds as the FRQTPA one. Not all the 22 loads are assigned frequency relays, the regulation for the existing ones are presented in Table 3.17.

Table 3.17 – Under frequency regulation for loads.

Bus ID	ID	FLSP [Hz]	FPPT [s]	Fraction	TB [s]	Amount Shed WV [MW]	Amount Shed SP [MW]
SEMF3	2	49	2,0	1	0,08	2,938	5,086
SEFO3	2	49	2,0	1	0,08	0,170	0,265
SESR1	1	49	3,0	1	0,08	3,290	5,849
SEFO1	2	49	3,0	1	0,08	0,992	1,972
SELG3	2	49	3,0	1	0,08	0,614	1,776
SELG1	1	48	2,0	1	0,08	1,380	4,831
SEFO1	3	48	2,0	1	0,08	0,464	0,859
SEMF3	3	48	4,0	1	0,08	1,224	2,544
SEFO3	3	48	4,0	1	0,08	0,792	1,539
SEFO1	1	48	5,0	1	0,08	1,418	2,452
SEFO3	1	48	5,0	1	0,08	1,467	2,275
SEPD1	2	47	4,0	1	0,08	1,165	3,369
SEPD1	3	47	5,0	1	0,08	2,886	7,180
SEPD1	4	47	5,0	1	0,08	2,250	7,732

In the previous table *FLSP* symbolizes the first load shedding point, *FPPT* the first point pickup time, *TB* the breaker opening time and *Fraction* represents the amount of load to shed, which is chosen as 100% for all the relays. The two last columns represent the amount of load active power that would be shed if constant load power characteristics were assumed during dynamic simulations.

Chapter 4 - Hydraulic Speed Governor Tuning

The dynamic performance of a system subjected to an islanding condition, that is, when groups of generators, lines and loads become isolated from each other, is broadly dependent on the performance of generators speed governing systems and on the action of frequency protection schemes. The main problem in frequency regulation for hydro plants arises due to conflicting governor response requirements for stable operation under isolated or system islanding conditions and for load variations under synchronous operating conditions. The islanding condition means that the hydraulic power plant has to manage power system frequency on its own, while on normal synchronous operating conditions, frequency control is exerted by all generation units with speed governors incorporated. Although fast governor response is desirable when rapid load changes occur, its corresponding settings may cause frequency instability when the system is under islanding conditions. A hydraulic unit in isolated operation is consequently the most critical condition for establishing governor requirements [7].

4.1 Linear Model Analysis

The convenient approach to study hydro governor behaviour in isolated operation is to start by performing an eigenvalue analysis on the linear model presented in chapter 2. This analysis is adequate to observe the effects of variations in certain parameters on the stability of frequency oscillations.

The linear model of Figure 2.13, adapted to consider load changes, is implemented with MATLAB. Figure 4.1 illustrates this model, where all signals are given in per unit. Notice that mechanical starting time M and load damping coefficient D , correspond to the variables T_M and K_D in that model of Figure 2.13.

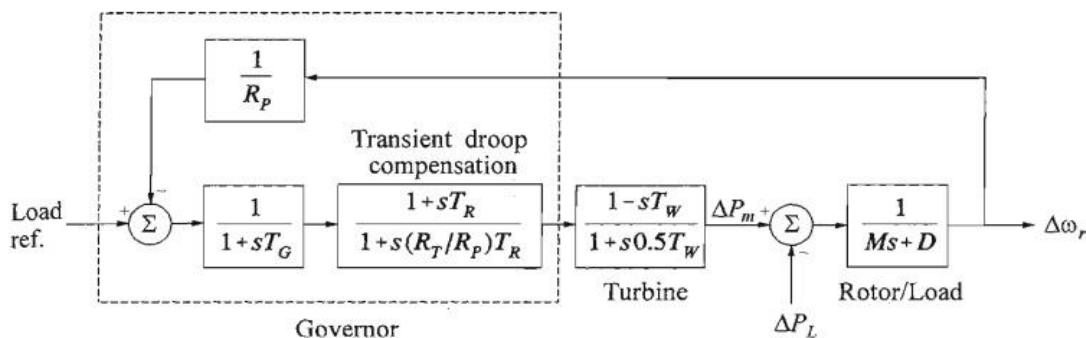


Figure 4.1 – Hydraulic unit speed governor block diagram.

In order to optimize the performance of the speed governor of Figure 4.1, the parameters dashpot reset time T_R and the temporary droop R_T , can be varied. The effects of varying these two parameters are studied for units with different values of water time constant T_W and mechanical starting time T_M .

The performance factors analysed, based on the eigenvalue technique, are the time constants corresponding to real eigenvalues and the damping ratios corresponding to complex eigenvalues. As known from systems theory, the response of a linear system is a linear combination of its modes, which are defined by the eigenvalues and corresponding eigenvectors. For a real eigenvalue $\lambda = \sigma$, its time constant is simply given by

$$T_\lambda = -1/\sigma \quad (4.1)$$

while for a complex eigenvalue $\lambda = \sigma \pm jw$, where the real component represents damping and the imaginary component gives the damped frequency of oscillation, the damping ratio is expressed as

$$\xi = \frac{-\sigma}{\sqrt{\sigma^2 + w^2}} \quad (4.2)$$

The set of parameters chosen to perform the first simulation is expressed in Table 4.1

Table 4.1 – Base governor parameters.

T_w [s]	T_M [s]	Kd	T_g [s]	Rp
2,0	6,0	1,0	0,2	0,05

The value of K_d , which as indicated before represents the load damping, is assumed to be 1, to account for the variation of load power with the network's frequency. The effects that varying the parameters T_R and R_T have on the performance factors presented above are shown quantitatively in Table 4.2.

Table 4.2 – Effect of governor parameters for a unit with $T_w = 2,0$ and $T_M = 6,0$.

Governor Parameters		Eigen Values			Damp. Ratio	Time Constants [s]	
R_T	T_R [s]	Mode 1	Mode 2	Mode 3	Mode 1	Mode 2	Mode 3
0,40	2,0	0,121 ± j 0,549	-5,882	-0,589	-0,215	0,170	1,698
0,40	6,0	-0,049 ± j 0,606	-5,921	-0,167	0,082	0,169	6,00
0,40	10,0	-0,081 ± j 0,638	-5,929	-0,089	0,125	0,169	11,21
0,40	3,0	0,043 ± j 0,559	-5,902	-0,393	-0,077	0,169	2,544
0,55	3,0	-0,04 ± j 0,464	-5,586	-0,431	0,086	0,176	2,321
0,70	3,0	-0,08 ± j 0,389	-5,555	-0,476	0,201	0,180	2,101
0,60	2,0	0,026 ± j 0,450	-5,619	-0,640	-0,057	0,178	1,562
0,60	6,0	-0,181 ± j 0,475	-5,652	-0,167	0,357	0,177	6,00
0,60	10,0	-0,217 ± j 0,515	-5,658	-0,083	0,389	0,177	12,107
0,40	8,0	-0,07 ± j 0,625	-5,926	-0,117	0,111	0,169	8,584
0,55	8,0	-0,18 ± j 0,528	-5,707	-0,112	0,322	0,175	8,917
0,70	8,0	-0,248 ± j 0,447	-5,573	-0,107	0,485	0,179	9,313

As can be readily seen, the existence of three system modes, one being a pair of complex conjugate eigenvalues, is a direct result of the fact that we are dealing with a fourth-order system. Therefore, two time constants associated with the two real poles and the damping ratio corresponding to the pair of complex conjugate roots are determined to illustrate the overall nature of the problem. When the real part of the pair of complex eigenvalues is positive, evaluation of its damping ratio results in a negative value, which means the system undergoes instability through oscillations of increasing amplitude. This usually happens for small values of both T_R and R_T . Otherwise, for a negative real part, the system exhibits stability of its oscillations and increasingly so, the larger the negative component gets. The damping ratio ξ is therefore of primary importance to the stability and performance of the unit when in

isolated operation. The remaining modes, given by two real roots, translate into two time constants that characterize the response rate of the system. Time constant of mode 2 is associated with the real pole that is more distanced from the imaginary axis, in the complex plane, hence its lowest value. On the other hand, as the time constant of mode 3 exhibits larger values, improvement in the response rate of the governor is essentially covered by the reduction of this time constant. The process of optimizing governor parameters consists in finding a compromise between a well damped oscillation behaviour and an acceptable speed of response. From Table 4.2 the following conclusions, relating the choice of parameters T_R and R_T to their effects on the performance factors, can be taken:

- For the range of temporary droop R_T that is of interest, this parameter has a very small effect on the time constants of the system. In fact, for a fixed low value of T_R , increasing R_T speeds up the response of the system (by reducing time constant of mode 3) and for a fixed high value of T_R , increasing R_T slows down the response, as time constant of mode 3 increases. On the other hand, the impact on the damping ratio is visible, with an increase in R_T resulting in smaller oscillation behaviour.
- As for the dashpot reset time T_R , both the damping ratio of mode 1 and the time constant of mode 3 are strongly influenced by this parameter's fluctuation. Increasing this parameter is followed by an increase in both the damping ratio of mode 1 and the time constant of mode 3, the latter resulting in slower response speed.

In order to have a qualitatively idea to support the above analysis, Figure 4.2 depicts several time responses for some of the T_R and R_T combinations of Table 4.2.

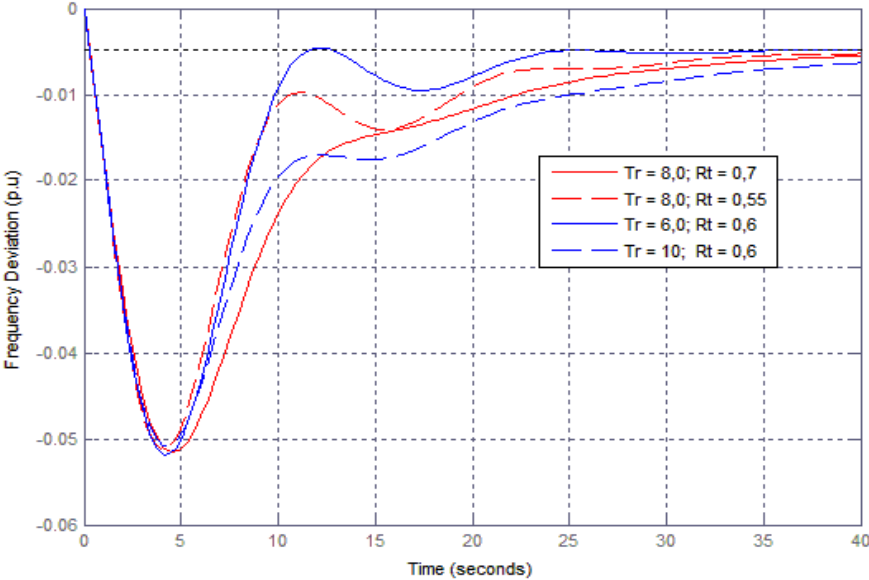


Figure 4.2 – Governor time simulations for a unit with $T_W = 2,0$ and $T_M = 6,0$.

The red coloured responses illustrate the effect of varying R_T for a fixed value of T_R . As expected, the red dashed response which has a lower R_T value, exhibits a more pronounced oscillating behaviour. The blue coloured responses reflect the effect of varying T_R for a fixed value of R_T . The blue solid lined

response is characterized by a larger damping ratio and at the same time a slightly faster rate of response, as a direct consequence of a lower T_R value than the blue dashed response.

While the results of Table 4.2 and Figure 4.2 are sufficient to illustrate the general idea behind speed governor performance optimization, a more suitable way of extending the analysis, in order to cover a wider variation of parameters, is to determine the loci of damping ratio and time constants. Essentially a locus represents a set of points whose location satisfies a specific condition. As has been constated both the damping ratio and the time constants are functions of the parameters R_T and T_R , hence, it is possible to represent curves along which these performance factors are constant, in a T_R - R_T plane. The locus representing the contour lines for the condition of constant damping ratio, for a unit with those parameters of Table 4.1, is shown in Figure 4.3.

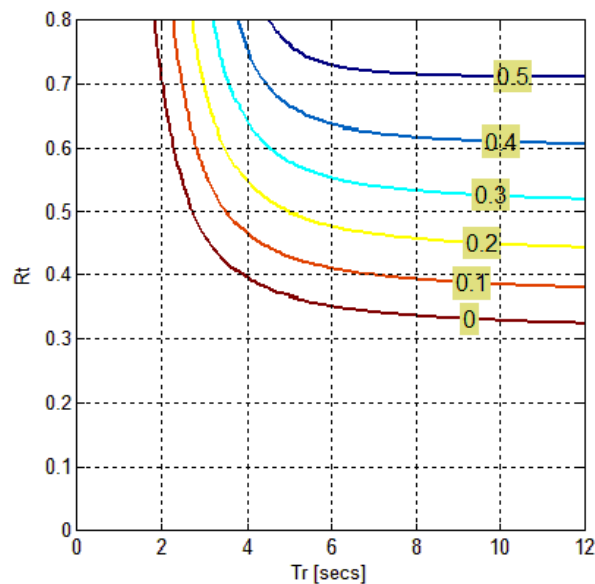


Figure 4.3 – Constant damping ratio locus for a unit with $T_W = 2,0$ and $T_M = 6,0$.

The contour line representation in Figure 4.3 indicates that the system only becomes stable for values of R_T larger than about 0,3 and for values of T_R larger than about 1,5. This is acknowledged by having in mind that for values of damping ratio larger than zero, the system is stable, while for negative values of damping ratio the system is unstable. For $\xi = 0$ the system is said to be marginally stable. Although both parameters influence the damping ratio, as seen before, when increasing them above a certain threshold, approximately 8 for T_R and 0,8 for R_T , the effect starts becoming negligible. Increasing them would only slow down the rate of response.

Despite the fact that the performance factor, damping ratio ξ , is of fundamental importance for governor tuning, it is of equal interest to represent the locus for the conditions of constant time constant of mode 2 and constant time constant of mode 3. These are shown in Figure 4.4 and Figure 4.5 respectively.

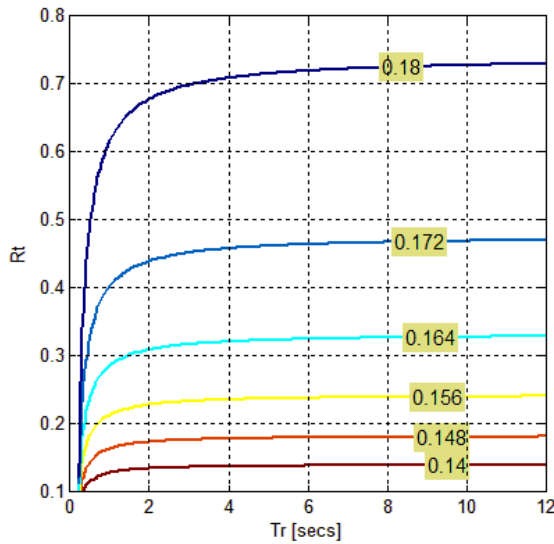


Figure 4.4 - Constant time constant of mode 2 locus for a unit with $T_W = 2,0$ and $T_M = 6,0$.

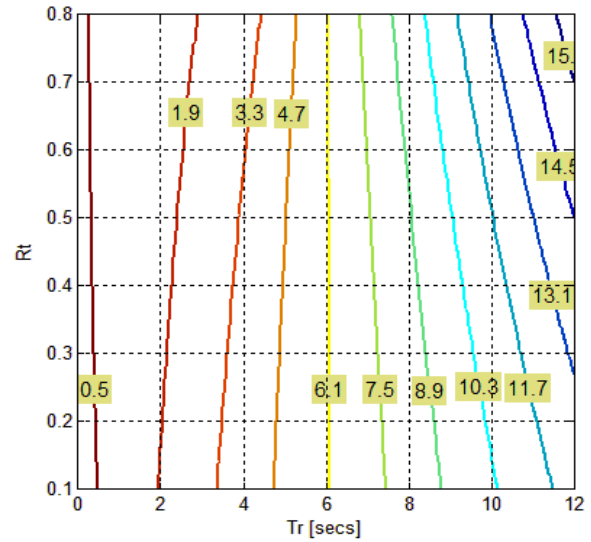


Figure 4.5 - Constant time constant of mode 3 locus for a unit with $T_W = 2,0$ and $T_M = 6,0$.

The loci above suggest that each time constant is influenced almost exclusively by one of the variables in play. A predominant effect of R_T on time constant of mode 2 is visible, for the range of relevant T_R values, while the influence of T_R is nearly irrelevant. Concerning the time constant of mode 3, which is the most important of the two, its greater influence comes from the parameter T_R . As for R_T , two distinct behaviours are observed. For low values of T_R , increasing R_T has the effect of increasing the time constant, while for higher values of T_R the opposite is true.

The previous analysis is extended in order to cover other combinations of water time constant T_W and mechanical starting time T_M , as these are the hydro plant related variables that most influence a unit's performance. Illustrations of constant damping ratio loci for variations of these parameters are shown from Figure 4.6 to Figure 4.8.

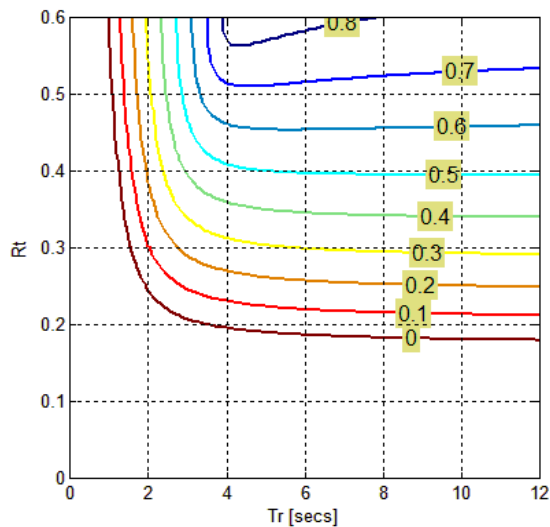


Figure 4.6 - Constant damping ratio locus for a unit with $T_W = 1,0$ and $T_M = 6,0$.

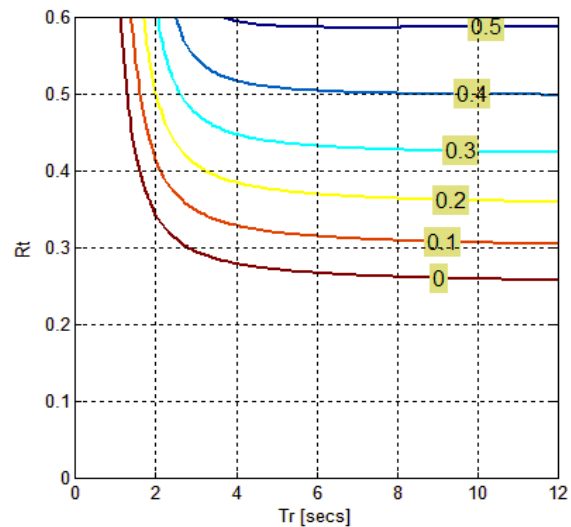


Figure 4.7 - Constant damping ratio locus for a unit with $T_W = 1,0$ and $T_M = 4,0$.

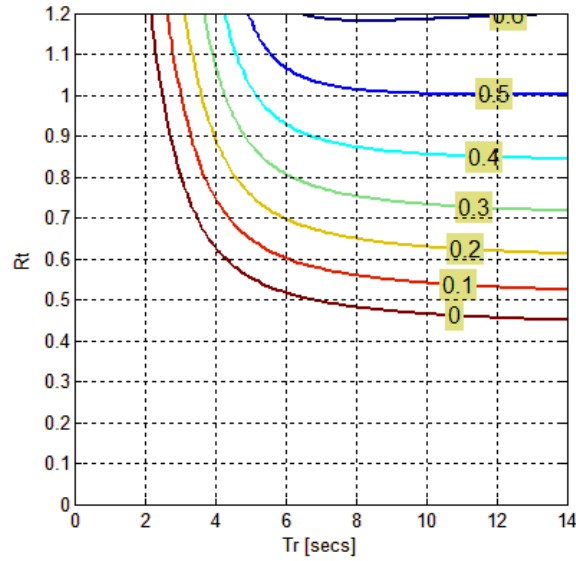


Figure 4.8 - Constant damping ratio locus for a unit with $T_W = 3,0$ and $T_M = 6,0$.

The results from the last three figures allow two different comparisons to be made. The locus in Figure 4.7 differs from that of Figure 4.6 by a reduction in the mechanical starting time T_M , which is accompanied by a contraction in the stability margin of the system, that is, the contour lines exhibit a slight shift in the direction of increasing R_T . The impact this shift has on the study of the optimum performance of the system is the increase of the parameters R_T and T_R in order to maintain an adequate value of damping ratio. On the other hand, Figure 4.8 represents the locus for a unit with $T_W = 3,0$, which is higher than the T_W of the unit in Figure 4.6. This reveals a similar behaviour of the contour lines, as observed in the previous comparison, although while in the first case it occurs by a reduction of T_M , in the second case it is an increase in T_W that causes the contraction of the stability margin.

The linear model analysis presented so far suggests that relationships exist between optimum choices of T_R and R_T with unit parameters machine starting time T_M and water time constant T_W , as seen in the previous loci of constant damping ratio. Although explicit formulas could be obtained for these functions, a rather different approach is taken in this work. Optimum choice of parameters is presented in the next section for the nonlinear model mentioned in chapter 3, the HYGOV model, by performing governor simulations and improving the frequency stability following a trial and error method. Nevertheless, two formulas pertaining to the linear model are presented here, which were developed by P. Kundur in his work [7]:

$$T_R = (5 - (T_W - 1) \times 0.5) \times T_W \quad (4.3)$$

$$R_T = (2.3 - (T_W - 1) \times 0.15) \times \frac{T_W}{T_M} \quad (4.4)$$

Equations (4.3) and (4.4) show that the dashpot reset time T_R depends solely on T_W , while the temporary droop R_T depends on both T_W and T_M . In the next section, it is acknowledged that T_R should also be adjusted when T_M fluctuates and the results given from these equations are confronted with the results obtained by the trial and error optimization.

4.2 HYGOV Model Analysis

While equations (4.3) and (4.4) were obtained by P. Kundur having the linear model as a basis, relationships between those parameters are established in this work by making use of the nonlinear model, which was introduced in chapter 2 as the combination of the models of Figure 2.12 and Figure 2.5. This model is present in PSS/E's library as HYGOV, its block diagram is shown in Figure 4.9.

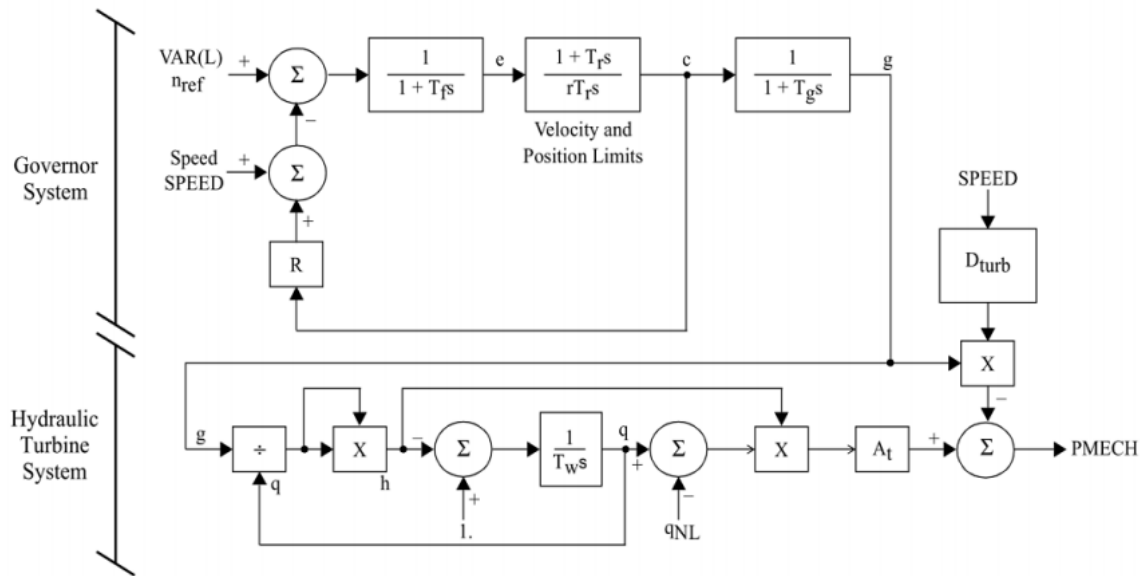


Figure 4.9 – Nonlinear HYGOV model block diagram [8].

The figure above was taken from the PSS/E manuals and a different convention is observed for some of the parameters. Parameter r stands for what has been referred to as the temporary droop R_T , parameter R is the same as the permanent droop R_p and parameter T_f corresponds to T_p , the pilot valve time constant. The parameters that remain unchanged throughout the simulations are given in Table 4.3. The fact that a Pelton turbine is assumed in the simulation is accounted for in the value of D_{turb} . A Francis turbine, on the other hand, usually has $D_{turb} = 0,5$. VELM represents the absolute maximum gate movement velocity.

Table 4.3 – Fixed HYGOV parameters.

VELM [1/s]	Gmin [p.u]	Gmax [p.u]	Dturb	At	Tf [s]	Tg [s]	Rp
0,0333	0,07	1,0	2,0	0,86	0,05	0,2	0,05

Governor simulations are performed assuming there is a load step change in the unit and observing how the speed governor controls the frequency and the mechanical power of the unit. The load step change is an increase of 10% of the unit's power capacity. It is also assumed that the unit is initially generating 70% of its nominal power, which is how these tests should usually be performed [9]. Figure 4.10 and Figure 4.11 depict the speed of the unit and its mechanical power responses, respectively, when varying the governor parameters T_R and R_T , for a unit with $T_M = 2 \times 1,435$ and $T_W = 0,89$.

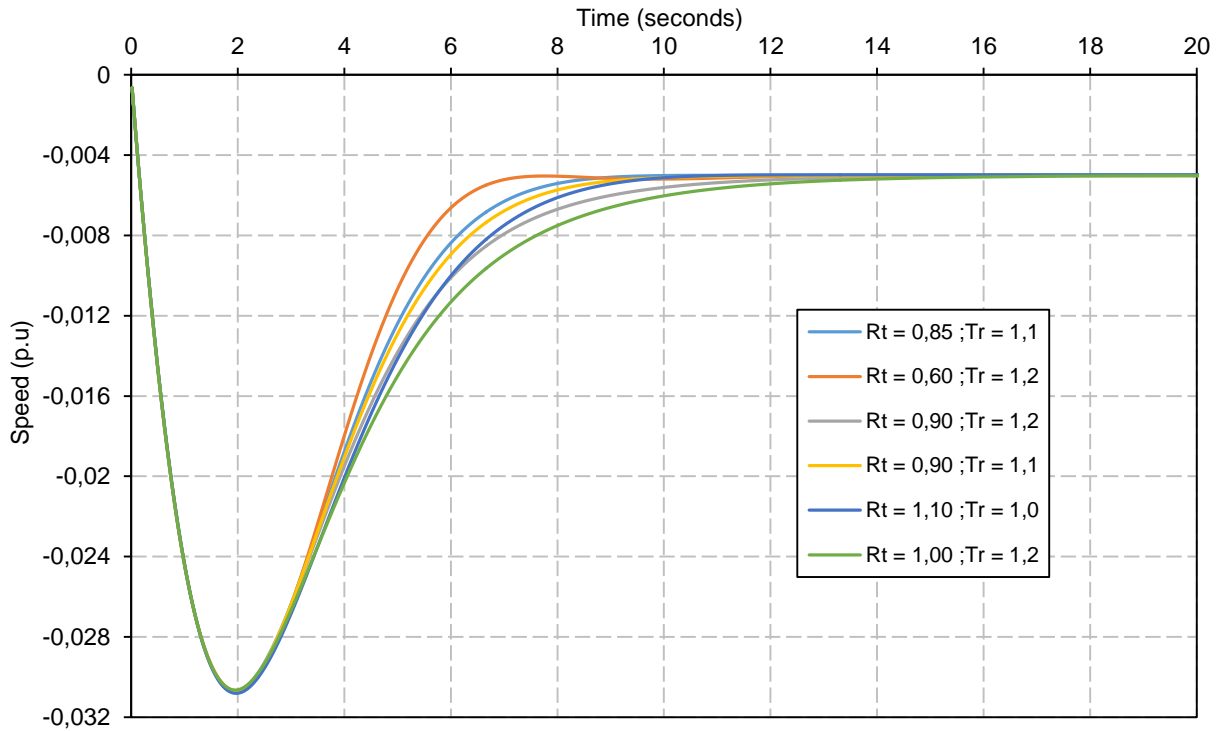


Figure 4.10 – Time simulations of speed for a unit with $T_M = 2 \times 1,435$ and $T_W = 0,89$.

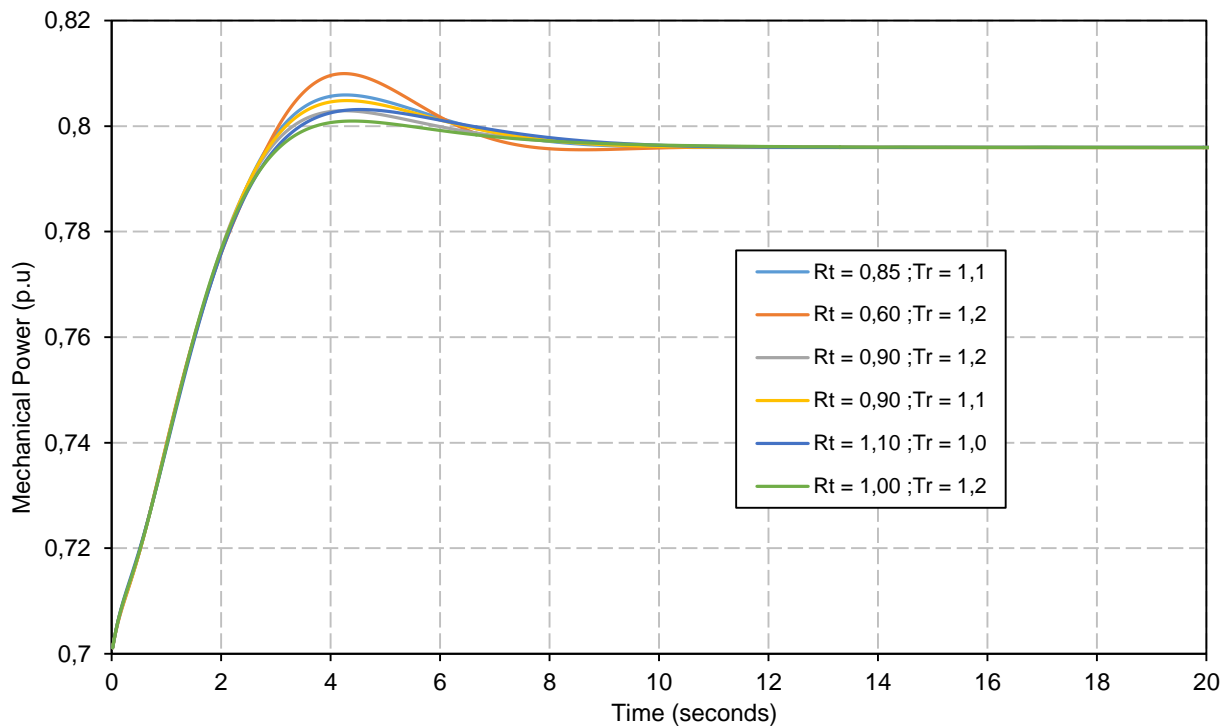


Figure 4.11 – Time simulations of mechanical power for a unit with $T_M = 2 \times 1,435$ and $T_W = 0,89$.

The results in the figures above expose the general idea behind trial and error optimization. It was performed through observation of the speed oscillations of the unit, upon experiments with different combinations of parameters R_T and T_R . Close observation of Figure 4.10 reveals that the light blue curve with $R_T = 0,85$ and $T_R = 1,1$, is the optimum choice. All the other curves, except for the red coloured one with $R_T = 0,60$ and $T_R = 1,2$, exhibit a slightly lower rate of response. Although the curve with $R_T = 0,60$

and $T_R = 1,2$ is faster, a small overshoot appears between $t = 6$ and $t = 8$ seconds, hence, it is not considered an optimum response. For these same sets of parameters, mechanical power responses for this particular unit are shown to depict a peak overshoot in each test. This phenomenon is not critical for governor optimization purposes and therefore it has no impact on the choice of R_T and T_R .

Simulations of the same nature as the above are extended to cover units with different values of T_M and T_W . A summary of the results is presented in Table 4.4, where the optimum choices obtained by simulating the nonlinear model HYGOV are confronted with the optimum choices calculated by using P. Kundur's equations (4.3) and (4.4).

Table 4.4 – Optimum parameters choices for several units.

Unit Parameters		HYGOV optimum parameters		P. Kundur optimum parameters	
T_W [s]	T_M [s]	R_T	T_R [s]	R_T	T_R [s]
0,89	2,0	1,00	0,9	1,03	4,5
0,89	2,87	0,85	1,1	0,72	4,5
0,89	4,0	0,52	1,5	0,52	4,5
0,89	6,0	0,34	2,0	0,34	4,5
0,89	8,0	0,24	2,4	0,26	4,5
0,89	10,0	0,16	2,5	0,21	4,5
0,89	12,0	0,12	2,5	0,17	4,5
1,0	2,87	0,78	1,2	0,80	5,0
2,0	2,87	1,07	1,5	1,49	9,0
3,0	2,87	1,24	1,8	2,09	12,0
4,0	2,87	1,26	2,2	2,58	14,0

The case in Table 4.4 highlighted in bold matches that of Figure 4.10 and Figure 4.11, which corresponds to the machine and site parameters to be used in the network simulations of chapter 5. As mentioned before, when performing trial and error optimization on the HYGOV model, not only the parameter R_T needs to be adjusted but also T_R . This is immediately observed, as an increase in both T_W and T_M is accompanied by an increase in the dashpot reset time constant T_R . The same does not happen when calculating the optimum parameters with Kundur formulas, as only a variation in T_W causes a variation in T_R . The temporary droop R_T follows the same pattern in both optimization approaches, an increase of T_M causes a decrease of R_T while an increase of T_W is followed by an increase in R_T . This proportional relationship between T_W and R_T is a direct consequence of the effect that opening the gate of the turbine has on delaying the flow of water through it. Augmenting T_W has the impact of making this effect more pronounced, contributing to stronger oscillations of the mechanical power and therefore the speed of the unit. Ultimately, increasing R_T softens this effect as higher values equal higher damping of response. Speed responses comparing the influence of optimum parameters by both methods are shown in Figure 4.12, for the highlighted case in Table 4.4 and for the last case of the same table.

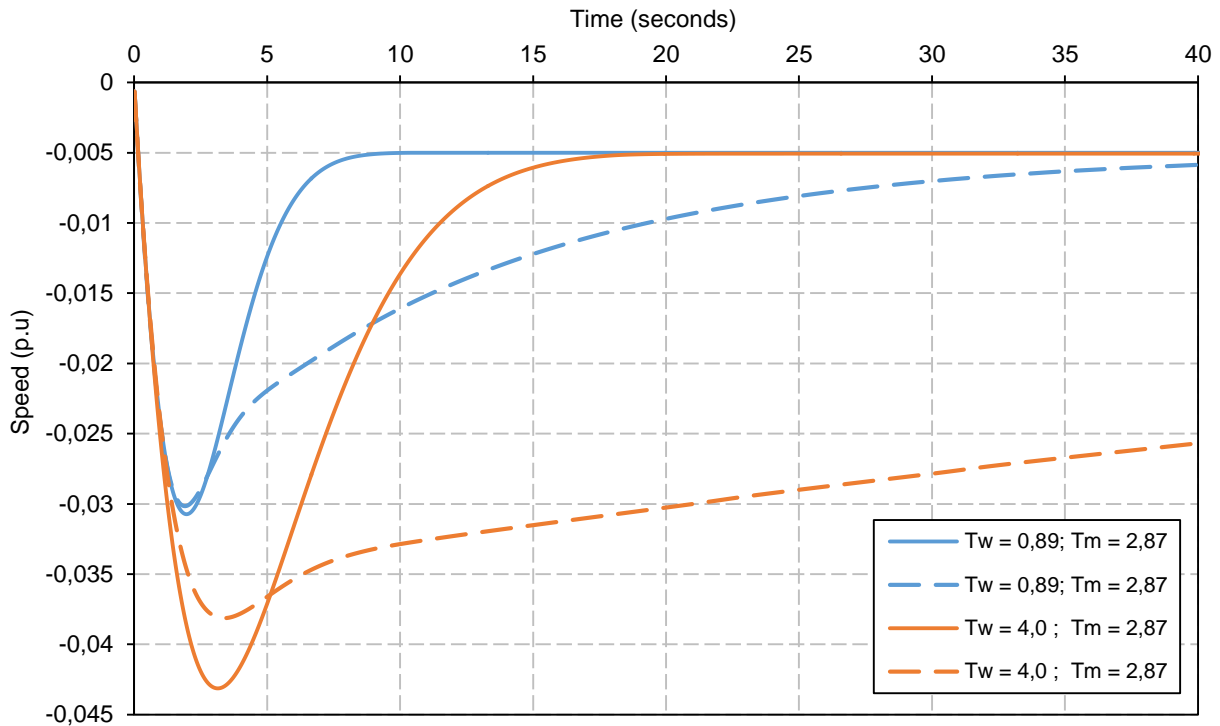


Figure 4.12 – Optimum dynamic speed responses for two cases.

The purpose of Figure 4.12 is to show how the two methods of parameter optimization influence the speed responses of the unit. In both cases, the dashed curves represent the responses when parameters obtained by Kundur formulas are used, while the solid line curves depict the responses obtained by using the parameters from trial and error simulation. For the unit with $T_W = 0,89$ and $T_M = 2,87$, while the optimum temporary droop R_T from both methods is similar, T_R obtained by trial and error simulations is much lower than Kundur's, which causes the response to reach steady state faster. Identical behaviour occurs for the case with $T_W = 4,0$ and $T_M = 2,87$, although the difference in T_R is much larger. Another effect, already described above, can be observed here, which is the increase of T_W and the subsequent enhancement of the system oscillations. The maximum speed deviation in transient state is higher for the case with $T_W = 4,0$, and despite the fact that R_T can mitigate the overshoot after the first oscillation, no change in either R_T or T_R can reduce the peak value of that first oscillation, without compromising an adequate responsiveness of the system.

As T_W represents a construction site parameter, it is held fixed from the beginning of the hydro plant project. At best, one possible way to mitigate the effect that higher values of T_W have on the first oscillation of the governor response, would be to increase the machine starting time T_M . Naturally, the lower this parameter the cheaper the unit's generator will be, as T_M is proportional to the moment of inertia of the machine and consequently its mass. The effect that increasing T_M has on the governor response for a fixed value of T_W is demonstrated in Figure 4.13.

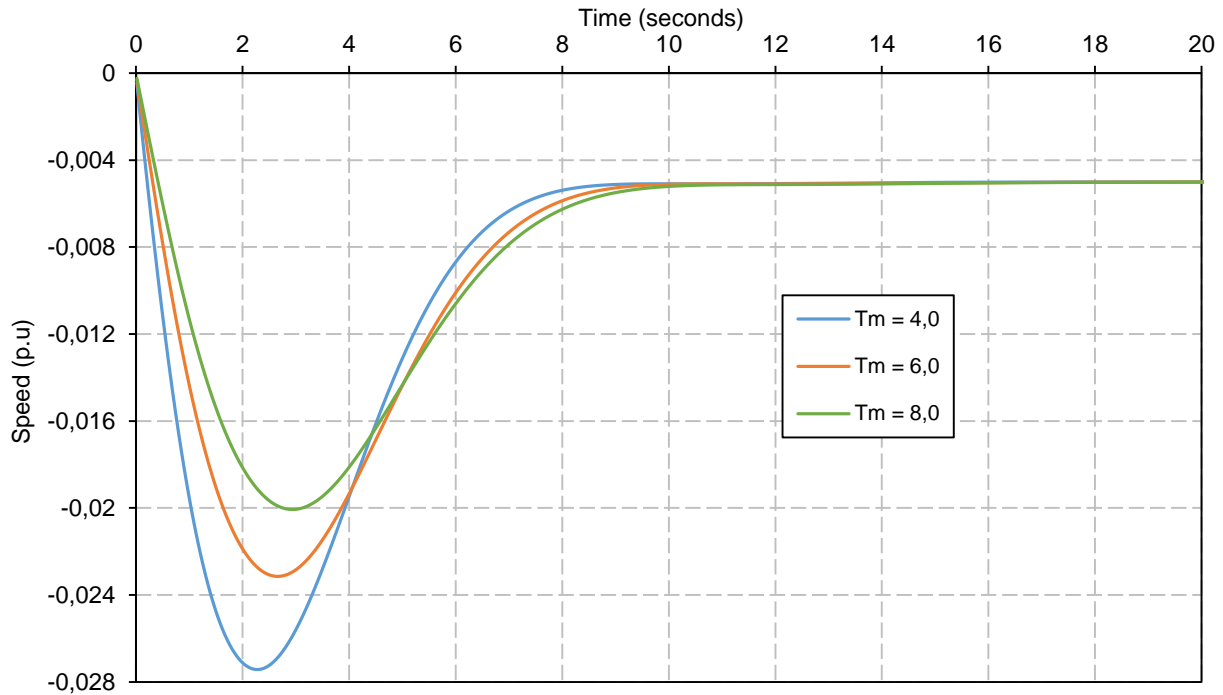


Figure 4.13 – Effect of unit parameter T_M in speed governor response.

Even if the first oscillation gets steeper for larger values of T_W , the responses in Figure 4.13 are obtained for the unit with $T_W = 0,89$. The validity of what is being analysed is not affected due to this option, as the purpose is to simply observe the effect of T_M on the system responses. For each of the responses, the chosen values of R_T and T_R are the optimum ones obtained by the trial and error optimization as in Table 4.4. The impact of increasing T_M is clear, for this case raising this time constant from 4,0 to 8,0 causes a reduction of about 30% in the maximum frequency deviation, while slightly slowing down the speed of response as the time to reach the steady state goes up.

So far in this section, the focus has been on the analysis of the performance of a Pelton turbine. In order to have an idea on how the speed responses of hydro units compare with the one of a thermal unit, Figure 4.14 shows speed governor simulations for three different units. The response of a Pelton equipped unit, with the optimum parameters computed before, the response of one large unit of the Caldeirão power plant and the response of a Francis equipped hydro unit are compared. The model employed to simulate a hydro unit equipped with a Francis turbine is the same that has been used for the Pelton turbine, the HYGGOV model, with the exception that for a Francis turbine the parameter D_{turb} takes a value of 0,5. The unit parameters T_W and T_M in the highlighted case of Table 4.4 are assumed for both Pelton and Francis turbines. Governor parameters T_R and R_T are taken to be the optimum ones, which for the Pelton turbine can be found in Table 4.4 and for the Francis turbine, performing the same trial and error optimization, are $T_R = 2,1$ and $R_T = 0,8$.

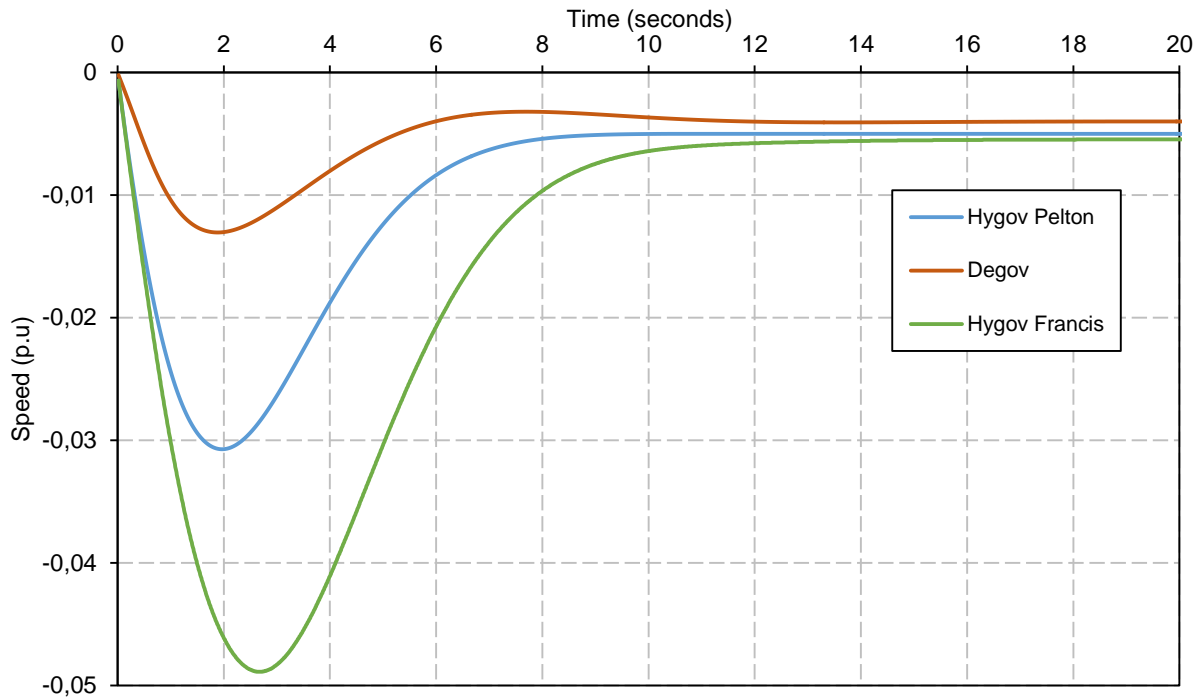


Figure 4.14 – Speed governor responses of hydro and thermal units.

Figure 4.14 exposes the behaviour of the speed governors of the units simulated. The fact that the maximum speed deviation is less pronounced in a thermal unit and the relatively fast speed of response, makes it the common choice for power system frequency regulation. Although a hydro unit with the optimum set of governor parameters can exhibit a competitive speed of response, the increased maximum speed deviation makes the hydro unit less capable of dealing with frequency regulation. The second fact to be noted is the strong influence of the parameter D_{turb} , which takes a low value for the Francis turbine, causing the maximum speed deviation to be more pronounced for this type of turbine.

The last thing to be added about this section is that, as previously mentioned, all the simulations were performed by considering the unit initially supplying 70% of its nominal power and subjected to a load step change of 10%. It is well known that nonlinear models are sensitive to initial conditions and the size of the disturbances, which means different test conditions would cause the choice of optimum parameters to change. Still, the chosen conditions represent a situation of nearly full generation capacity upon the load step increase and therefore are suitable for the analysis.

Chapter 5 - Network Dynamic Simulations

This chapter deals with the analysis of the impact that the Furnas hydroelectric power plant has on the primary frequency regulation of the São Miguel power system. The dynamic simulations of the grid are performed using the software PSS/E, as previously noted. PSS/E uses a second order Euler numerical integration algorithm, an explicit method, to solve the nonlinear equations. In order to avoid numerical instability problems, the integration time step needs to be kept smaller than about 1/5 to 1/4 of the shortest time constant in the system being simulated. For this specific case, an integration time step of 1 *ms* is chosen.

Given the São Miguel power system a series of contingencies are simulated independently, which are chosen in accordance with incidents information provided by EDA. The selected contingencies are:

- Foros 60kV/30kV transformer fault in the winter valley scenario. Transient behaviour of the grid is compared for a situation where the hydro speed governors are considered with a situation where only the thermal unit speed governor is in service.
- Pico Vermelho power plant contingency, causing it to disconnect from the grid. Analysis is performed for both winter valley and summer peak scenarios, with and without the consideration of the hydro speed governors. Additionally this contingency is studied when load shedding is not considered.
- Caldeirão unit 5 contingency studied for the winter valley scenario. Again, both cases with and without the consideration of hydro speed governors are inspected.
- Caldeirão unit 6 transformer contingency studied for the summer peak scenario. Analysis is made with and without considering load shedding.
- The Pico Vermelho power plant contingency for the summer peak scenario. The purpose in this case is to compare the performances of Pelton turbines with the ones of Francis turbines.

The initial conditions for each study are shown in chapter 3, as power flow results for both scenarios. The load shedding assumed for all the cases and the motor frequency protection schemes are presented in Table 3.17 and Table 3.16, respectively, in chapter 3. A symmetric short circuit is the standard fault assumed for the dynamic simulations, which occurs at $t = 0,1 s$ and is cleared 100 *ms* after, followed by the tripping of the faulted element. Reclosing is not considered.

5.1 Foros 60kV/30kV Transformer Fault

The contingency of the 60kV/30kV transformer in Foros substation is analysed for the winter valley scenario. The initial conditions pertaining to this scenario, injected active and reactive power by the dispatched power plants, are shown in Table 5.1.

Table 5.1 – Foros 60kV/30kV transformer contingency initial conditions.

	Injected Active Power [MW]	Injected Reactive Power [Mvar]
Graminhais	2,73	0
Ribeira Grande	13,00	0
Pico Vermelho	16,00	0
Waste Incineration	3,80	0
Furnas	-10,00	3,89
Caldeirão	9,92	6,99
Total	35,45	10,89

The fault is a three phase short circuit happening at $t = 0,1 s$, lasting until $t = 0,2 s$, as it is assumed that the protection takes a total of $100 ms$ to eliminate the fault, taking the transformer out of service. The result is that the load connected to the 30kV bus prior to the fault is now disconnected, which accounts for a load loss of 2,43 MW and 0,6 Mvar. The chosen bus to observe frequency regulation by the speed governors in the system is the Caldeirão power plant 60kV bus, which is shown in Figure 5.1. The response CTCL6 (A) is related to the situation that considers the two hydro speed governors in service, while the response CTCL6 (B) represents the assumption of constant mechanical power for the hydro units, that is, exclusion of those speed governors.

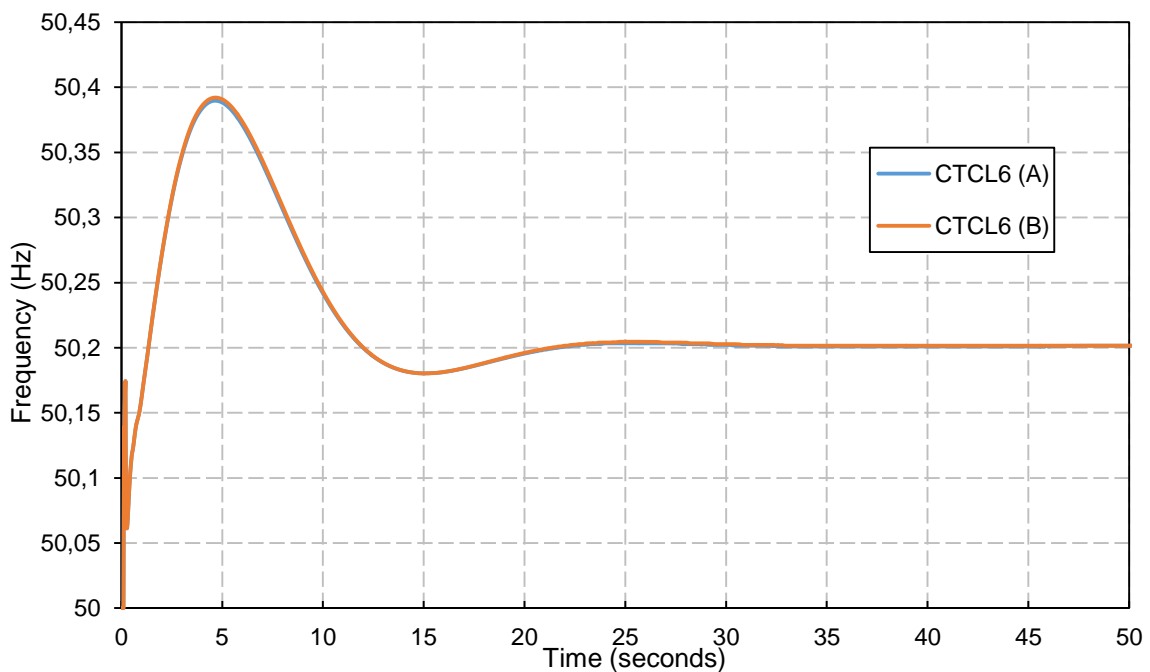


Figure 5.1 – Frequency response on the 60kV bus of the Caldeirão power plant for the Foros transformer fault. CTCL6 (A) – HYGOV considered. CTCL6 (B) – HYGOV not considered.

Responses for both cases are very similar, as seen in Figure 5.1. The frequency regulation is almost entirely assumed by the Caldeirão unit, DEGOV model, which is a direct consequence of the low strength of the contingency. No load nor motor shedding occur in this situation, as we are dealing with an over frequency response.

It is also interesting to inspect the behaviour of the mechanical power of the units responsible for the frequency regulation. Figure 5.2 illustrates these variables for the group 5 of the Caldeirão plant and group 1 of the Furnas hydro plant, for both A and B cases.

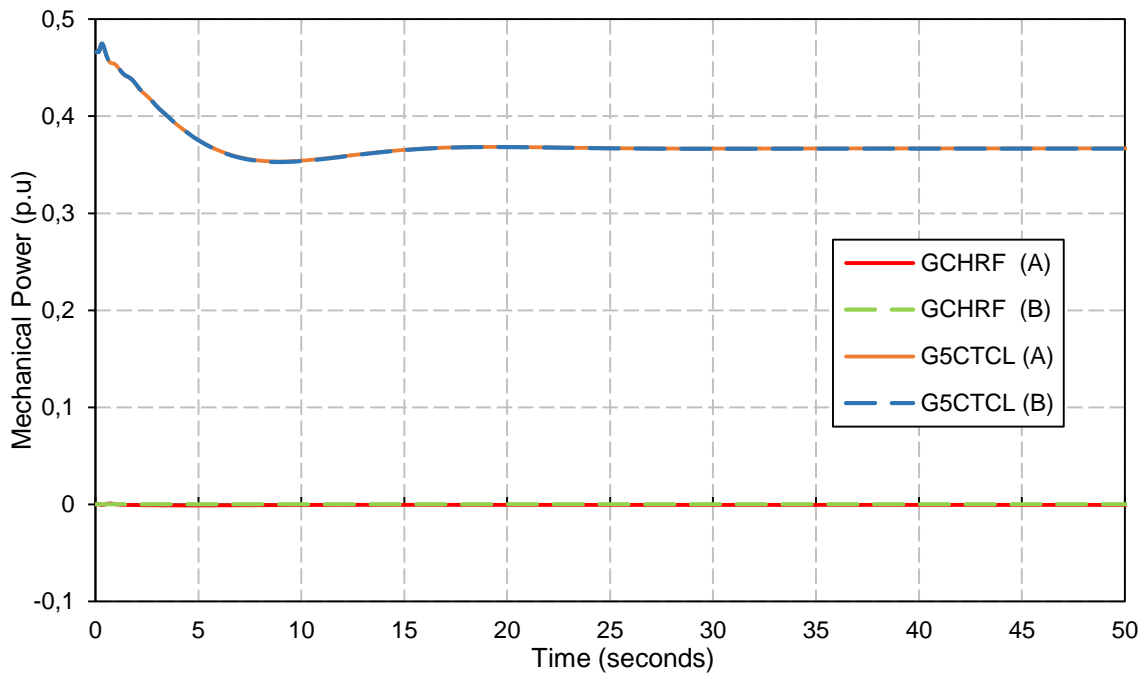


Figure 5.2 – Mechanical power response of the Caldeirão Unit 5 and the Furnas Unit 1 for the Foros transformer fault. GCHRF (A) and G5CTCL (A) – HYGOV considered. GCHRF (B) and G5CTCL (B) – HYGOV not considered.

Similarly to the frequency response of Figure 5.1, it is seen that the mechanical power behaviour for both cases is practically the same and DEGOV assumes the regulation.

5.2 Pico Vermelho Contingency

The contingency of the Pico Vermelho geothermal power plant is simulated for the winter valley and the summer peak scenarios. For both cases the fault is the three phase short circuit at $t = 0,1 s$, which is eliminated after $100 ms$, resulting in the tripping of both groups of this power plant. In both scenarios the power generated by this utility is the same, 16 MW and no reactive power, meaning the generation power lost due to this contingency is the same for both cases.

5.2.1 Summer Peak

For the summer peak scenario the initial conditions are expressed in Table 5.2.

Table 5.2 – Pico Vermelho summer peak contingency, initial conditions.

	Injected Active Power [MW]	Injected Reactive Power [Mvar]
Graminhais	2,73	0
Ribeira Grande	13,00	0
Pico Vermelho	16,00	0
Waste Incineration	6,70	0
Furnas	11,42	0,49
Caldeirão	27,27	27,43
Total	77,12	27,92

Again, frequency variation is observed on the 60 kV bus of the Caldeirão power plant, which is presented in Figure 5.3. CTCL6 (A) refers to the situation that considers the two hydro speed governors in service and load shedding active. CTCL6 (B) reflects the situation of exclusion of the hydro units speed governors and load shedding active. CTCL6 (C) is the same as CTCL6 (A) but with load shedding inactive and finally CTCL6 (D) is similar to CTCL6 (B) also with load shedding off.

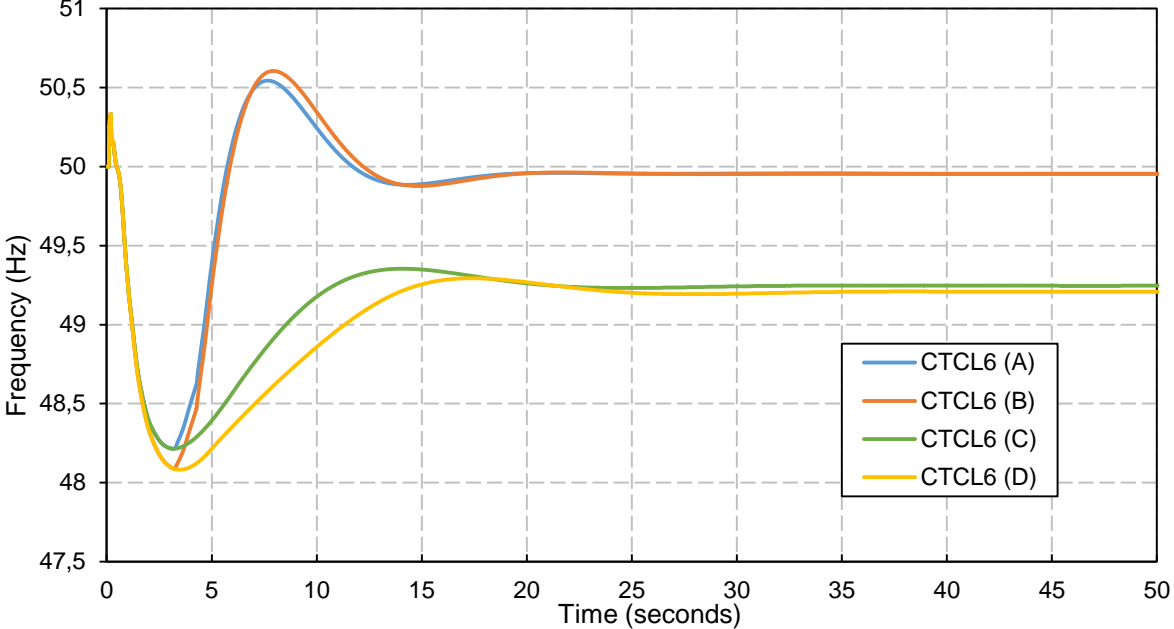


Figure 5.3 – Frequency response on the 60kV bus of the Caldeirão power plant for the Pico Vermelho contingency. CTCL6 (A) – HYGOV considered with load shedding ON. CTCL6 (B) – HYGOV not considered with load shedding ON. CTCL6 (C) – HYGOV considered with load shedding OFF. CTCL6 (D) – HYGOV not considered with load shedding OFF.

Figure 5.3 reveals that when load shedding is active, cases A and B exhibit similar behaviour, although the maximum transient frequency deviation is higher when hydro speed governors are not considered. A more pronounced difference exists between responses C and D, when load shedding is off, where it is visible that the inclusion of the hydro speed governors contributes significantly to frequency regulation. Naturally the steady state frequency deviation is larger when not considering load shedding, as the system speed governors have to control system frequency on their own. The sequence of the load relays operation for cases A and B is presented in Table 5.3.

Table 5.3 – Load relay operations for Pico Vermelho summer peak contingency.

Without Hydro Governors (case B)						
Bus ID	Load ID	t = 1,216 s	t = 3,216 s	t = 3,296 s	t = 4,216 s	t = 4,296 s
SESR1	1	Relay Start			Breaker Start	Load Shed
SEFO1	2	Relay Start			Breaker Start	Load Shed
SEMF3	2	Relay Start	Breaker Start	Load Shed		
SELG3	2	Relay Start			Breaker Start	Load Shed
SEFO3	2	Relay Start	Breaker Start	Load Shed		
With Hydro Governors (case A)						
Bus ID	Load ID	t = 1,227 s	t = 3,227 s	t = 3,307 s	t = 4,227 s	t = 4,307 s
SESR1	1	Relay Start			Breaker Start	Load Shed
SEFO1	2	Relay Start			Breaker Start	Load Shed
SEMF3	2	Relay Start	Breaker Start	Load Shed		
SELG3	2	Relay Start			Breaker Start	Load Shed
SEFO3	2	Relay Start	Breaker Start	Load Shed		

Observation of Table 5.3 reveals the same amount of load shed for both cases. Load shedding has a significant effect on frequency regulation as the final frequency deviation in Figure 5.3 is very close to the rated frequency, 50 Hz.

5.2.2 Winter Valley

For the winter valley scenario the initial conditions are expressed in Table 5.4. It should be noted that the contingency for this scenario results in a loss of generated power of almost 50%.

Table 5.4 – Pico Vermelho winter valley contingency, initial conditions.

	Injected Active Power [MW]	Injected Reactive Power [Mvar]
Graminhais	2,73	0
Ribeira Grande	13,00	0
Pico Vermelho	16,00	0
Waste Incineration	3,80	0
Furnas	-10,00	3,89
Caldeirão	9,92	6,99
Total	35,45	10,89

Frequency variation is observed on the 60 kV bus of the Caldeirão power plant, which is presented in Figure 5.4. CTCL6 (A) refers to the situation that considers the two hydro speed governors in service. CTCL6 (B) also reflects the situation that considers the hydro speed governors in service, but with Kundur optimum T_R and R_T parameters. CTCL6 (C) pertains to the situation that considers only the modelling of the thermal units speed governors.

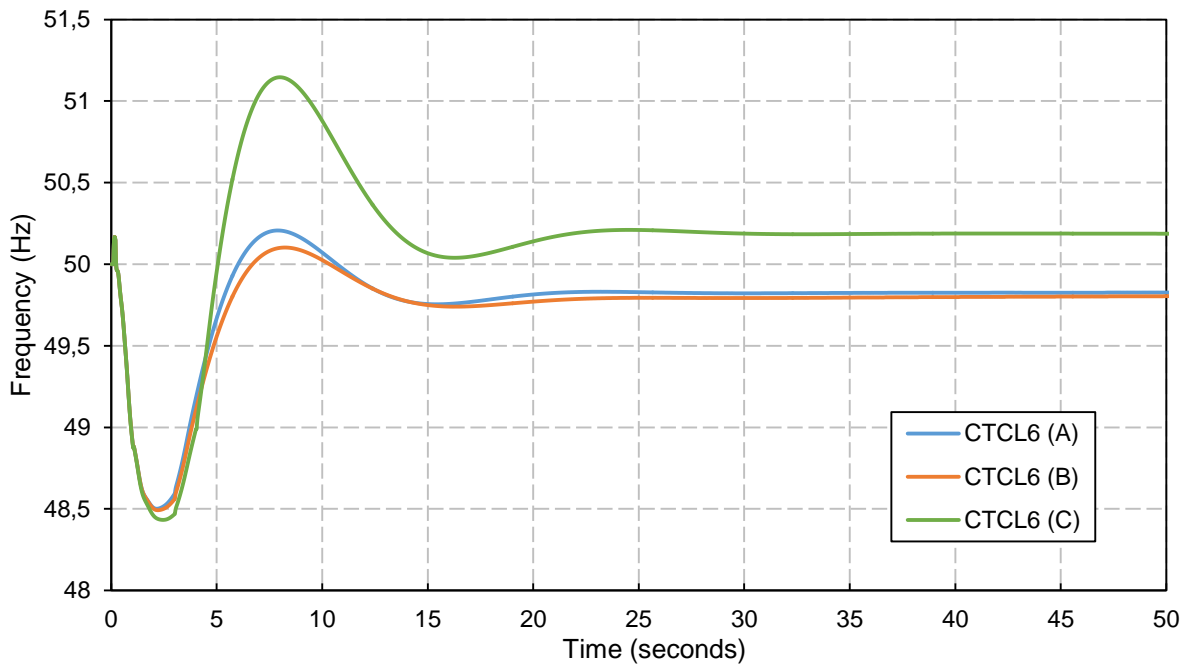


Figure 5.4 – Frequency response on the 60kV bus of the Caldeirão power plant for the Pico Vermelho contingency. CTCL6 (A) – HYGOV considered. CTCL6 (B) – HYGOV considered with Kundur optimum parameters. CTCL6 (C) – HYGOV not considered.

Despite the usual comparison between considering and not considering the hydro speed governors, Figure 5.4 includes the frequency response obtained when those speed governors are parameterized with Kundur optimum parameters. A slight delay of response is observed for case B, with Kundur parameters, compared to case A that uses governor parameters obtained by trial and error optimization. This is expected, as seen before in Figure 4.12 of chapter 4. The response for case C, which excludes hydro speed governors and stabilizes in a frequency value above 50 Hz. This is an indication that load shedding is larger for case C, which can be seen in Table 5.5.

Table 5.5 – Load relay operations for Pico Vermelho winter valley contingency.

Without Hydro Governors (case C)								
Bus ID	Load ID	t = 0,936 s	t = 0,956 s	t = 1,036 s	t = 2,936 s	t = 3,016 s	t = 3,936 s	t = 4,016 s
CHRF	-	Relay Start	Breaker Start	Pumps Shed				
SESR1	1	Relay Start					Breaker Start	Load Shed
SEFO1	2	Relay Start					Breaker Start	Load Shed
SEMF3	2	Relay Start			Breaker Start	Load Shed		
SELG3	2	Relay Start					Breaker Start	Load Shed
SEFO3	2	Relay Start			Breaker Start	Load Shed		
With Hydro Governors (case A)								
Bus ID	Load ID	t = 0,939 s	t = 0,959 s	t = 1,039 s	t = 2,939 s	t = 3,019 s	t = 3,709 s	
CHRF	-	Relay Start	Breaker Start	Pumps Shed				
SESR1	1	Relay Start					Relay Reset	
SEFO1	2	Relay Start					Relay Reset	
SEMF3	2	Relay Start			Breaker Start	Load Shed		
SELG3	2	Relay Start					Relay Reset	
SEFO3	2	Relay Start			Breaker Start	Load Shed		

Table 5.5 shows that when hydro speed governors are considered, at $t = 3,709 s$, frequency reaches a value higher than 49 Hz causing some of the protections to turn off, therefore not shedding the corresponding load.

Figure 5.5 illustrates mechanical power responses for the group 5 of the Caldeirão plant and group 1 of the Furnas hydro plant, for the case that considers the hydro speed governors and the case that does not consider these governors.

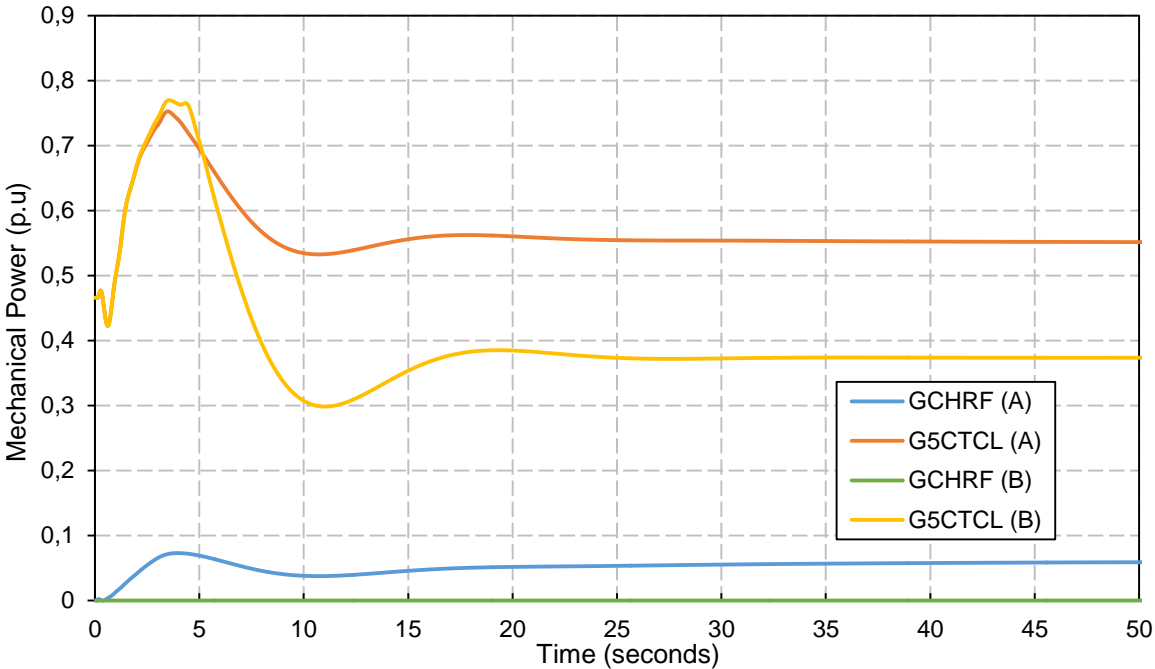


Figure 5.5 – Mechanical power response of the Caldeirão Unit 5 and the Furnas Unit 1 for the Pico Vermelho contingency. GCHRF (A) and G5CTCL (A) – HYGOV considered. GCHRF (B) and G5CTCL (B) – HYGOV not considered.

Figure 5.5 reveals that the actuation of the hydro speed governors in case A in the first time instants, contributes for a more controlled frequency response and less steep maximum transient frequency deviation.

Simulation of this contingency was also performed when not considering load shedding. Hydro pumps protections, on the other hand, were still considered to be active. The results for frequency variations in the 60 kV bus of the Caldeirão power plant are shown in Figure 5.6.

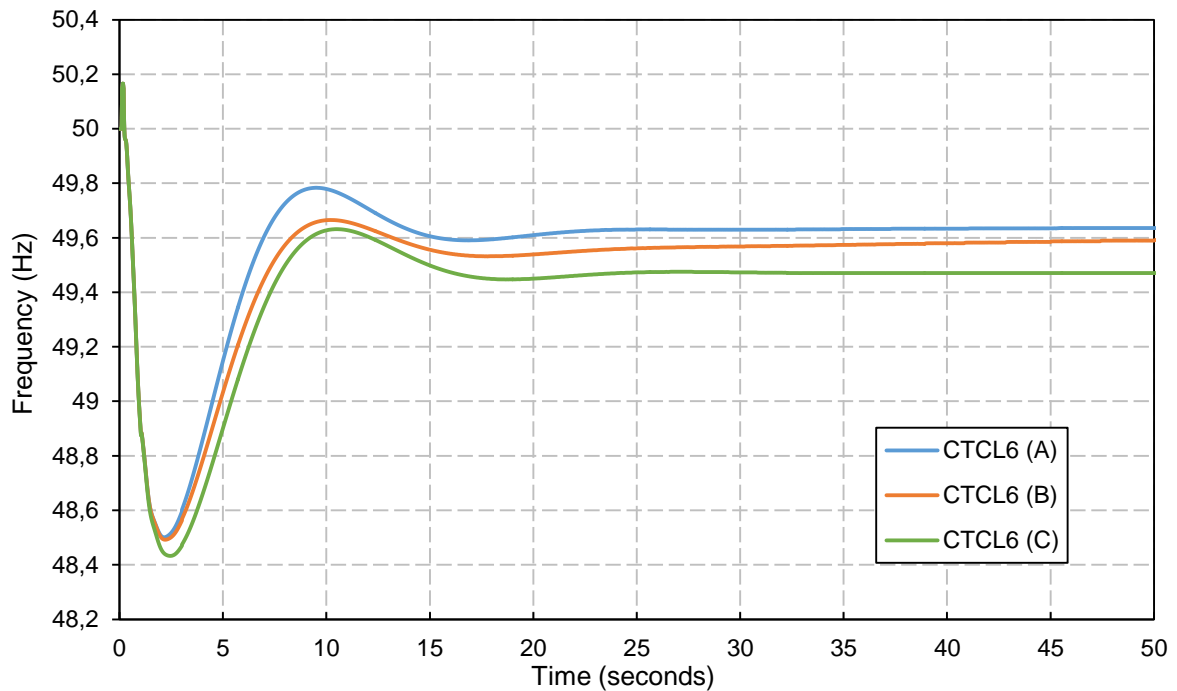


Figure 5.6 – Frequency response on the 60kV bus of the Caldeirão power plant for the Pico Vermelho contingency considering load shedding off. CTCL6 (A) – HYGOV considered. CTCL6 (B) – HYGOV considered with Kundur optimum parameters. CTCL6 (C) – HYGOV not considered.

As expected, when load shedding is not considered, the steady state frequency deviations are more pronounced. For all three cases only the shedding of the hydro power plant motors occur. The beneficial contribution of the hydro governing system for frequency regulation (cases A and B), is reflected in a smaller final frequency deviation and less steep maximum transient frequency deviation in the first 5 seconds of the responses. It should also be noted that when the hydro governor models are used with Kundur optimum parameters, case B, the time to reach the steady state is much larger than that of the remaining cases.

Lastly, the effect of the mechanical starting time T_M of the hydro units on frequency regulation is analysed. Simulations are made for 4 cases, with two different values of T_M and considering and not considering load shedding. Results of frequency responses in the 60 kV bus of the Caldeirão power plant for these 4 cases are presented in Figure 5.7.

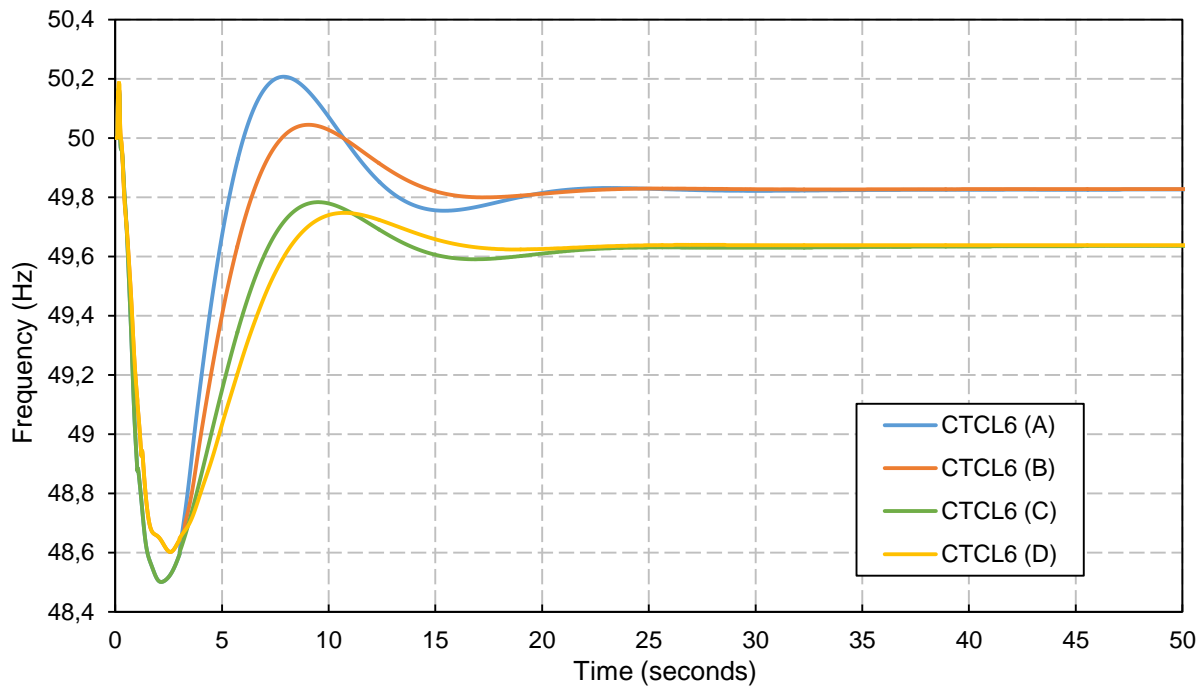


Figure 5.7 – Frequency response on the 60kV bus of the Caldeirão power plant for the Pico Vermelho contingency. CTCL6 (A) – Hydro unit with $T_M = 2,87$ and load shedding ON. CTCL6 (B) – Hydro unit with $T_M = 12$ and load shedding ON. CTCL6 (C) – Hydro unit with $T_M = 2,87$ and load shedding OFF. CTCL6 (D) – Hydro unit with $T_M = 12$ and load shedding OFF.

For the situation when load shedding is considered, cases A and B, Figure 5.7 reveals that a higher value of T_M causes the response to be slightly less oscillating, although more delayed. When load shedding is not considered, the difference is not as pronounced. These results confirm the ones presented in Figure 4.13 in chapter 4.

5.3 Caldeirão Unit 5 Contingency

The contingency of the Caldeirão Unit 5 is analysed for the winter valley scenario. The initial conditions pertaining to this scenario are shown in Table 5.6.

Table 5.6 – Caldeirão Unit 5 contingency initial conditions.

	Injected Active Power [MW]	Injected Reactive Power [Mvar]
Graminhais	2,73	0
Ribeira Grande	13,00	0
Pico Vermelho	16,00	0
Waste Incineration	3,80	0
Furnas	-10,00	3,89
Caldeirão	9,92	6,99
Total	35,45	10,89

The fault is the three phase short circuit happening at $t = 0,1 s$, lasting until $t = 0,2 s$, as it is assumed that the protection takes a total of $100 ms$ to eliminate the fault, taking the unit out of service originating a loss of $9,92 MW$ of generation power. This unit tripping makes the hydroelectric power plant the only one capable of performing primary frequency regulation. Frequency variation is observed on the $60 kV$

bus of the Caldeirão power plant, which is presented in Figure 5.8. Three cases are compared. CTCL6 (A) refers to the situation that considers the two hydro speed governors in service. CTCL6 (B) also reflects the situation that considers the hydro speed governors in service, but with Kundur optimum T_R and R_T parameters. CTCL6 (C) pertains to the situation that does not consider the inclusion of hydro speed governors, which means frequency regulation is assured by load shedding on its own.

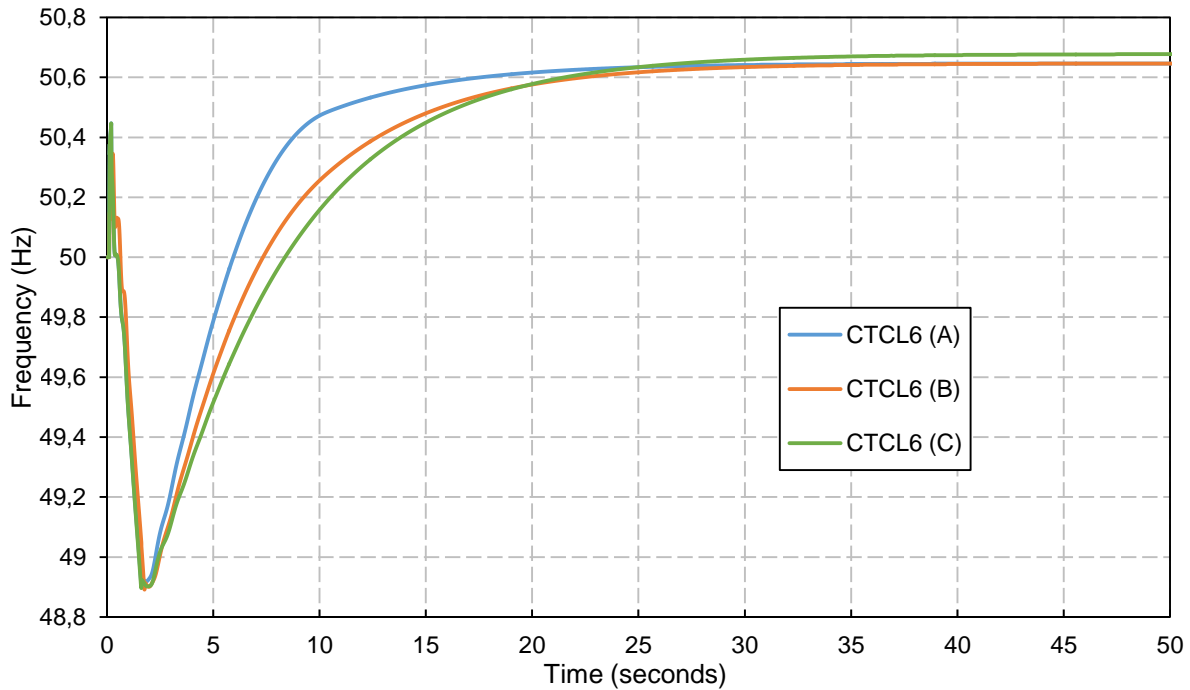


Figure 5.8 – Frequency response on the 60kV bus of the Caldeirão power plant for the Caldeirão Unit 5 contingency. CTCL6 (A) – HYGOV considered. CTCL6 (B) – HYGOV considered with Kundur optimum parameters. CTCL6 (C) – HYGOV not considered.

Figure 5.8 reflects that the response obtained by using the trial and error optimum parameters in the hydro speed governors is slightly faster than the remaining two. Additionally, the amount of load shedding is the same for all cases, which can be verified by Table 5.7.

Table 5.7 – Load relay operations for Caldeirão Unit 5 contingency.

Without Hydro Governors (case C)						
Bus ID	Load ID	t = 1,504 s	t = 1,507 s	t = 1,527 s	t = 1,607 s	t = 2,422 s
CHRF	-		Relay Start	Breaker Start	Pumps Shed	
SESR1	1	Relay Start				Relay Reset
SEFO1	2	Relay Start				Relay Reset
SEMF3	2	Relay Start				Relay Reset
SELG3	2	Relay Start				Relay Reset
SEFO3	2	Relay Start				Relay Reset
With Hydro Governors (case A)						
Bus ID	Load ID	t = 1,517 s	t = 1,52 s	t = 1,54 s	t = 1,62 s	t = 2,281 s
CHRF	-		Relay Start	Breaker Start	Pumps Shed	
SESR1	1	Relay Start				Relay Reset
SEFO1	2	Relay Start				Relay Reset
SEMF3	2	Relay Start				Relay Reset
SELG3	2	Relay Start				Relay Reset
SEFO3	2	Relay Start				Relay Reset

Table 5.7 shows that the hydro pumps' shedding is enough in order for the network to achieve a stable steady state value of the frequency.

Lastly, mechanical power responses for the three cases simulated are presented in Figure 5.9.

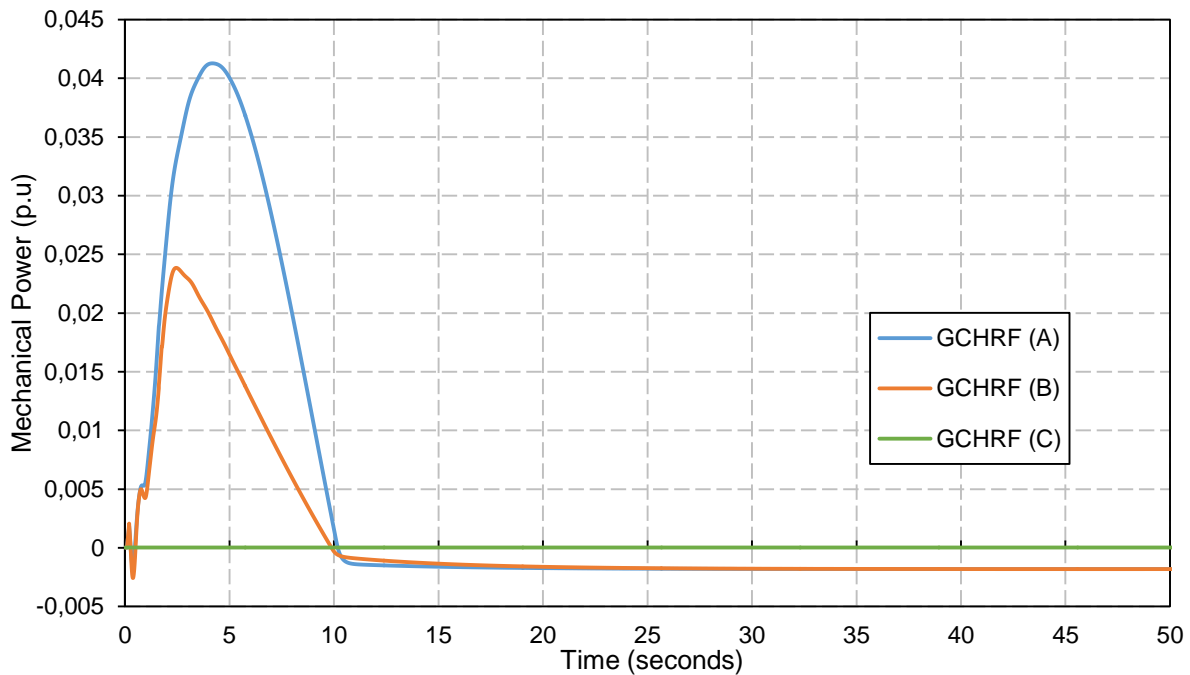


Figure 5.9 – Mechanical power responses of the Furnas Unit 1 for the Caldeirão Unit 5 fault. GCHRF (A) – Hydro governor with trial and error optimum parameters. GCHRF (B) – Hydro governor with Kundur optimum parameters. GCHRF (C) – Hydro governor not considered.

Figure 5.9 shows the impact that lower governor parameters, case A, have on the first oscillation of the mechanical power of the unit.

5.4 Caldeirão Unit 6 Transformer Contingency

The contingency of the Caldeirão Unit 6 transformer is analysed for the summer peak scenario. The initial conditions pertaining to this scenario are shown in Table 5.8.

Table 5.8 – Caldeirão Unit 6 transformer contingency initial conditions.

	Injected Active Power [MW]	Injected Reactive Power [Mvar]
Graminhais	2,73	0
Ribeira Grande	13,00	0
Pico Vermelho	16,00	0
Waste Incineration	6,70	0
Furnas	11,42	0,49
Caldeirão	27,27	27,43
Total	77,12	27,92

The three phase short circuit occurs at $t = 0,1 s$ at the high voltage side of the transformer of unit 6. When $t = 0,2 s$ is reached, the protection eliminates the fault tripping the transformer and the group, originating a loss of 13,8 MW, the power that was being generated by this unit. Frequency variation is observed on the 60 kV bus of the Caldeirão power plant, which is presented in Figure 5.10. Four cases

are simulated. CTCL6 (A) refers to the situation that considers the two hydro speed governors in service and load shedding on. CTCL6 (B) also reflects the situation that considers the hydro speed governors in service, but with Kundur optimum T_R and R_T parameters, also with load shedding on. CTCL6 (C) and CTCL6 (D) are equivalent to cases A and B, respectively, with the exception that load shedding is off.

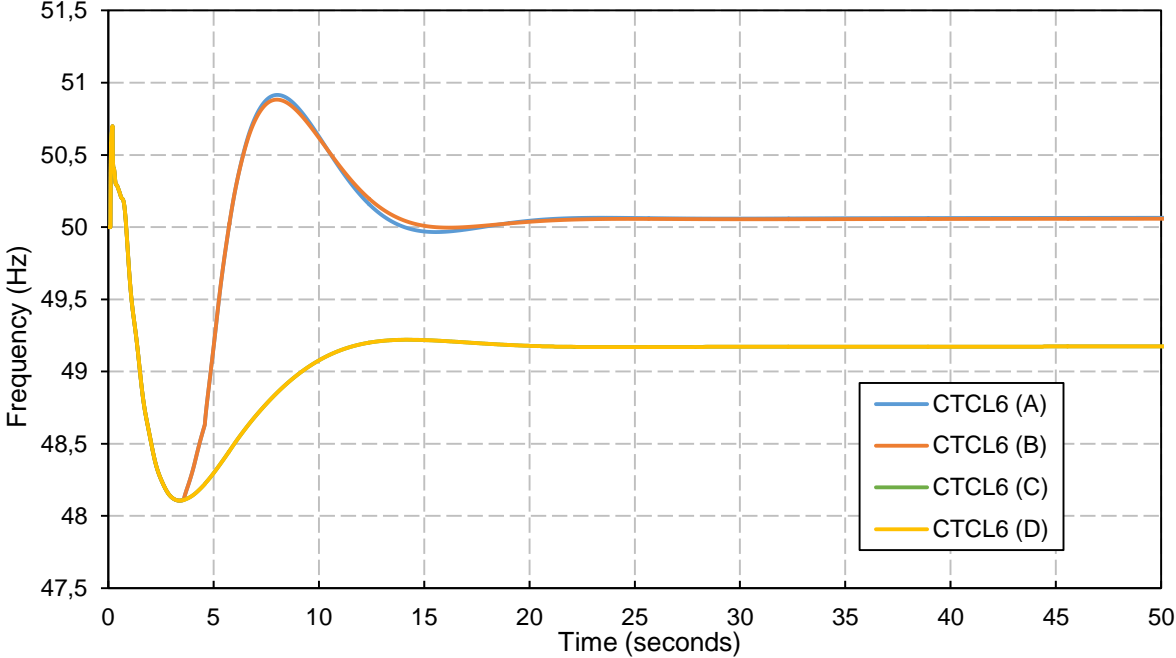


Figure 5.10 – Frequency response on the 60kV bus of the Caldeirão power plant for the Caldeirão Unit 6 transformer contingency. CTCL6 (A) – HYGOV considered with load shedding ON. CTCL6 (B) – HYGOV considered with Kundur optimum parameters and load shedding ON. CTCL6 (C) – HYGOV considered with load shedding OFF. CTCL6 (D) - HYGOV considered with Kundur optimum parameters and load shedding OFF.

Inspection of Figure 5.10 shows that for this contingency changing the hydro speed governor parameters has a minor impact in frequency regulation, especially when load shedding is not considered. For all the cases, the frequency steady state value is reached at about $t = 25 s$. For the two cases that assume load shedding as active, cases A and B, the sequence of load relay operations is shown in Table 5.9.

Table 5.9 – Load relay operations for Caldeirão Unit 6 transformer contingency.

Bus ID	Load ID	t = 1,504 s	t = 3,504 s	t = 3,584 s	t = 4,504 s	t = 4,584 s
SESR1	1	Relay Start			Breaker Start	Load Shed
SEFO1	2	Relay Start			Breaker Start	Load Shed
SEMF3	2	Relay Start	Breaker Start	Load Shed		
SELG3	2	Relay Start			Breaker Start	Load Shed
SEFO3	2	Relay Start	Breaker Start	Load Shed		

The table above reflects that the sequence of load relays operation is the same for the case that assumes the hydro governor parameters taken from trial and error optimization and the case that employs the use of Kundur optimum parameters.

Finally, mechanical power responses of the units responsible for frequency regulation which are in service are shown in Figure 5.11 and Figure 5.12. While the former pertains to the situation that considers load shedding active, the latter represents the case with load shedding inactive.

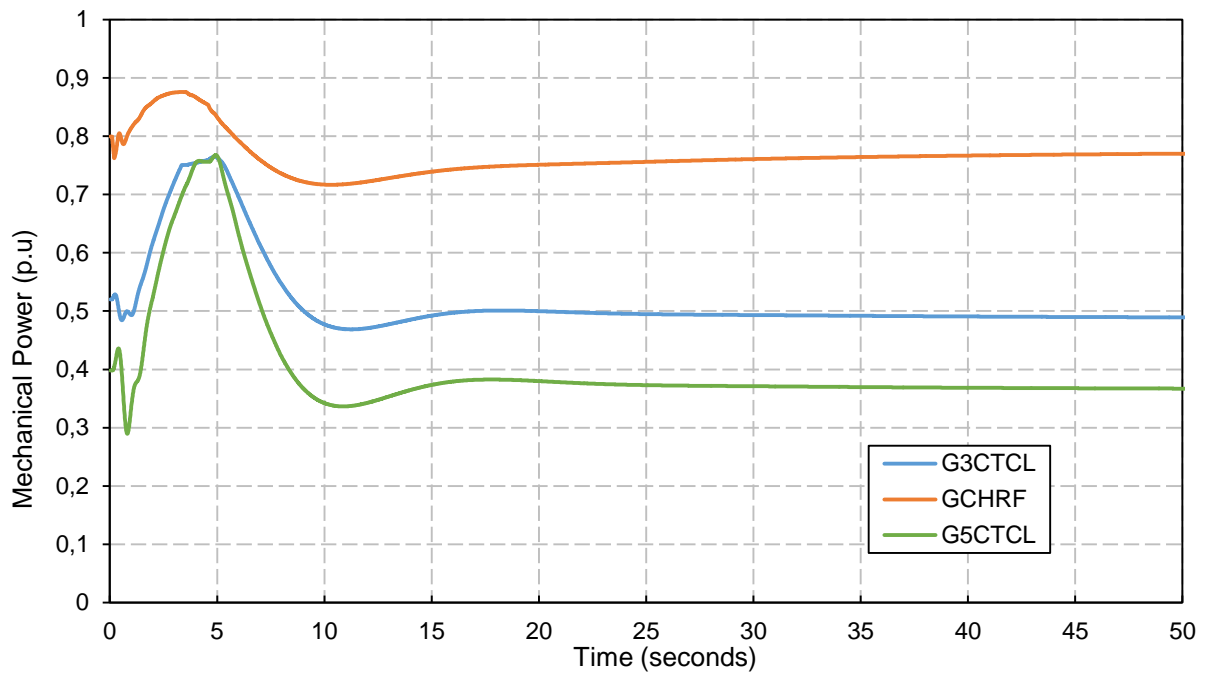


Figure 5.11 – Mechanical power responses of the Caldeirão Unit 3, the Furnas Unit 1 and the Caldeirão Unit 5 for the Caldeirão Unit 6 transformer contingency. Load shedding on.

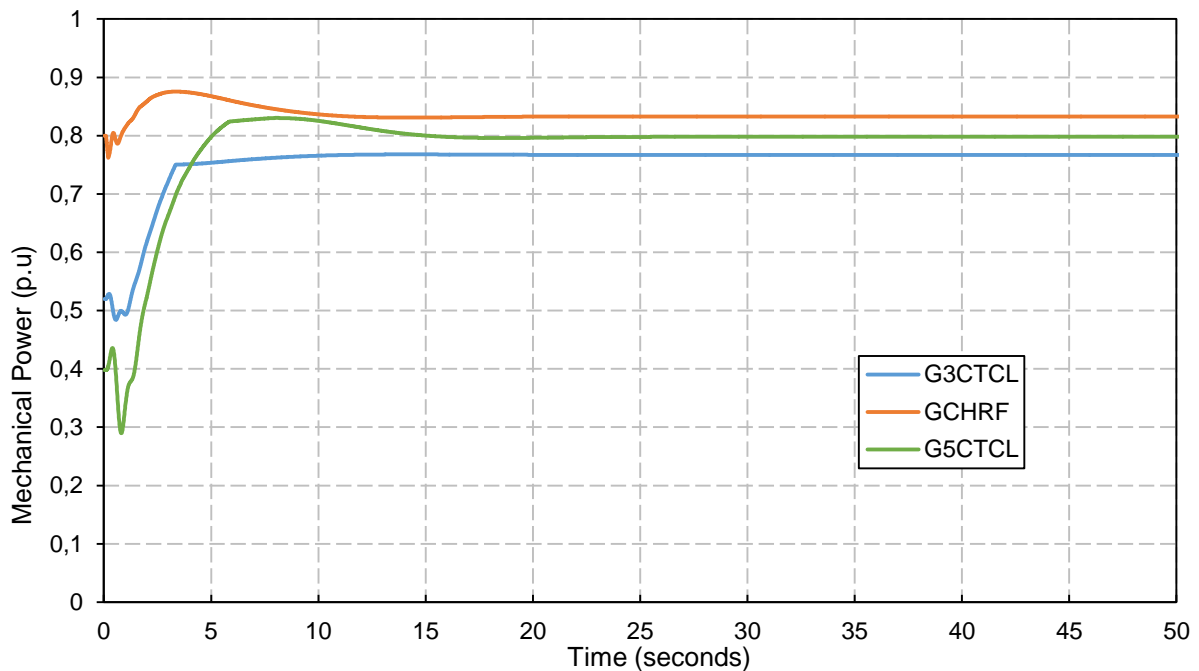


Figure 5.12 – Mechanical power responses of the Caldeirão Unit 3, the Furnas Unit 1 and the Caldeirão Unit 5 for the Caldeirão Unit 6 transformer contingency. Load shedding off.

The difference between the two figures is visible; when load shedding is on, its combination with the prime movers' frequency regulation results in a steady state value of the system frequency very close to 50 Hz. This also means the final mechanical power values of the units converge to values close to the ones prior to the contingency. When load shedding is off, it is up to the units to control system frequency on their own, resulting on final mechanical power values higher than those found prior to the fault.

5.5 Pelton vs Francis Performance

The purpose of this last sub-section is to get an idea of how the type of hydro turbine affects system frequency regulation when a fault occurs. The Pico Vermelho contingency from 5.2 in the summer peak scenario is chosen to achieve this comparison. Initial conditions are presented in Table 5.10

Table 5.10 – Initial conditions for the hydro turbine comparison case.

	Injected Active Power [MW]	Injected Reactive Power [Mvar]
Graminhais	2,73	0
Ribeira Grande	13,00	0
Pico Vermelho	16,00	0
Waste Incineration	6,70	0
Furnas	11,42	0,49
Caldeirão	27,27	27,43
Total	77,12	27,92

Frequency variation is observed on the 60 kV bus of the Caldeirão power plant, presented in Figure 5.13. Load shedding is not considered. CTCL6 (A) represents the situation with the hydro plant equipped with Francis turbines, while CTCL6 (B) corresponds to the already simulated case of the Pelton hydro turbines. The optimum governor parameters for the Francis turbines that were indicated in section 4.2 of chapter 4 are $T_R = 2,1$ and $R_T = 0,8$.

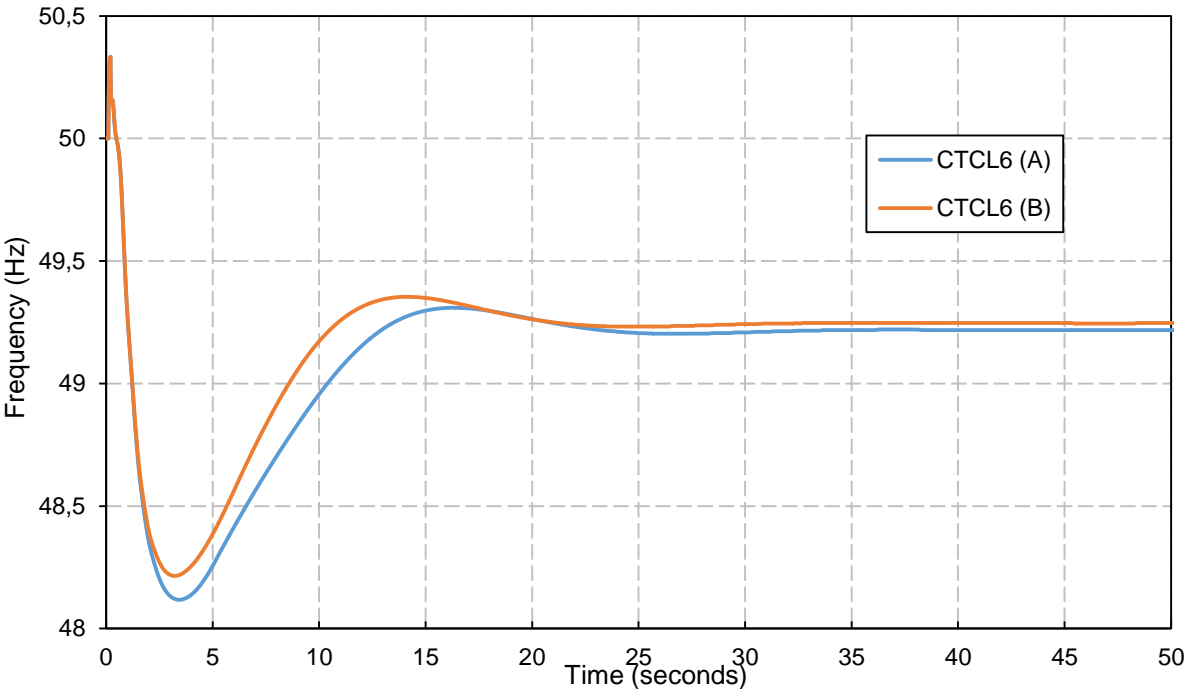


Figure 5.13 – Frequency response on the 60kV bus of the Caldeirão power plant for the Pico Vermelho contingency. CTCL6 (A) – HYGOV modelling a Francis turbine. CTCL6 (B) – HYGOV modelling a Pelton turbine. Load shedding is off.

The difference between the performances of the two turbines is visible. The fact that a Francis turbine has a lower turbine damping coefficient causes the response to be more oscillating and delayed. This confirms the results of Figure 4.14 in chapter 4.

Chapter 6 - Conclusion

6.1 Thesis Discussion

This thesis work dealt with the evaluation of a hydraulic power generating system performance in terms of frequency control, within an isolated power grid with a high share of wind power.

The first chapter introduced the general background of this work, highlighting the potential that hydroelectric power plants have, to compete with thermal power plants in frequency regulation, in a weak power system. After this, chapter 2 provided a review on relevant hydraulic turbines and speed governors models for this work's application. A linear model suitable for small perturbations analysis and a nonlinear model adequate to transient or large signal analysis were presented.

Chapter 3 was dedicated to describe the power network in which transient stability studies would be performed. Power flow results for two scenarios and dynamic models of the system's equipment were presented. Chapter 4 was focused on hydraulic speed governor analysis and tuning, considering the unit supplying an isolated load. The first section was aimed at understanding how changing speed governor settings affect the unit's frequency oscillations, by making use of the linear model. The second section concerned optimization of the nonlinear governor's response for several combinations of unit parameters.

Finally, the performance of the hydroelectric power plant with the optimum parameters determined in chapter 4, was evaluated in chapter 5. Several severe contingencies were simulated in the São Miguel power grid in order to examine primary frequency regulation. In addition a comparison between using a Pelton turbine and using a Francis turbine is made.

In short, the objectives proposed in chapter 1 were well accomplished. Although exact formulas relating the optimum hydraulic governor parameters T_R and R_T with the unit parameters T_W and T_M could not be determined, relationships, for their ranges of interest, were still found. The optimum parameters obtained by trial and error optimization of the HYGOV model were confronted with the optimum parameters suggested by Kundur in his paper. As Kundur optimum parameters are obtained by studying the linear model, their applicability when performing nonlinear simulations is limited and therefore, were found to be less accurate than the parameters obtained by trial and error optimization. This was then confirmed in chapter 5 for the contingencies of Pico Vermelho, in the winter valley scenario, and Caldeirão Unit 5, also in the winter valley scenario, where using Kundur optimum parameters slightly worsens the quality of the frequency response. Generally speaking, the results from chapter 5 reflect that the inclusion of the hydroelectric speed governors in situations when there is only one or no thermal speed governor in service (winter valley scenarios) is substantially more beneficial than in situations with more power generating capacity (summer peak scenarios) and thermal speed governors in service. This is also recognized when load shedding is off, no matter the amount of thermal generation. Overall, consideration of the hydroelectric speed governors led to slightly more damped first frequency oscillations and to higher rates of frequency stabilization. This is translated as a positive and desired impact of the hydroelectric speed governing devices in primary frequency control.

6.2 Future Work

Despite the positive results achieved with this work, there may still be room for further improvements. The speed governor used throughout the work relied on a PI control structure. PSS/E includes in its library a hydro governor model with proportional, integral and derivative control, the WEHGOV model. It represents the turbine as a nonlinear model for the penstock dynamics with no surge tank, similarly to the HYGGOV model. Therefore, it might be beneficial to use a speed governor with PID control action as a means to improve the performance of the hydroelectric power plant in primary frequency regulation.

In addition, the Pelton type of turbine was the main focus of the thesis. Although a study case considering the use of a Francis turbine instead of a Pelton one was presented, this type of analysis comparing turbine type performance could very well be extended. Simulations encompassing these two types of turbines and the Kaplan turbine could be performed in order to compare their performance.

Bibliography

- [1] P. Kundur, *Power System Stability and Control*, McGraw-Hill, 1994.
- [2] P. L. Dandeno, P. Kundur and J. P. Bayne, "Hydraulic Unit Dynamic Performance Under Normal and Islanding Conditions – Analysis and Validation," *IEEE Transactions on Power Apparatus and Systems*, Vols. PAS-97, pp. 2134-2143, 1978.
- [3] M. Eremia and M. Shahidehpour, *Handbook of Electrical Power System Dynamics*, John Wiley & Sons, 2013.
- [4] IEEE Committee Report, "Dynamic Models for Steam and Hydro Turbines in Power System Studies," *IEEE Transactions on Power Apparatus and Systems*, Vols. PAS-92, pp. 1904-1915, 1973.
- [5] Working Group on Prime Mover and Energy Supply Models for System Dynamic Performance Studies, "Hydraulic Turbine and Turbine Control Models for Dynamic Studies," *IEEE Transactions on Power Systems*, vol. 7, pp. 167-179, February 1992.
- [6] D. G. Ramey and J. W. Skooglund, "Detailed Hydrogovernor Representation For System Stability Studies," *IEEE Transactions on Power Apparatus and Systems*, Vols. PAS-89, pp. 106-112, January 1970.
- [7] R. A. Naghizadeh, S. Jazebi and B. Vahidi, "Modeling Hydro Power Plants and Tuning Hydro Governors as an Educational Guideline," *International Review on Modeling and Simulations*, vol. 5, pp. 1780-1790, 2012.
- [8] PSS/E, Model Library, October 2010.
- [9] PSS/E, Program Application Guide, Volume II, October 2010.
- [10] PSS/E, Program Operation Manual, October 2010.
- [11] PSS/E, Program Application Guide, Volume I, October 2010.
- [12] J. M. Undrill and J. L. Woodward, "Nonlinear Hydro Governing Model and Improved Calculation for Determining Temporary Droop," *IEEE Transactions on Power Apparatus and Systems*, Vols. PAS-86, pp. 443-453, April 1967.
- [13] J. L. Agüero, P. Arnera, M. B. Barbieri, M. C. Beroqui, R. E. B. Lastra, J. Mastronardi and R. Molina, "Hydraulic Transients in Hydropower Plant. Impact on Power System Dynamic Stability," *Power and Energy Society General Meeting*, 2008.

Appendix A – Grid schematic

